DEPARTMENT OF ECONOMICS
AND BUSINESS ECONOMICS
AARHUS UNIVERSITY

CREATES
Center for Research in Econometric Analysis of Time Series

Forecasting the Global Mean Sea Level, a Continuous-Time State-Space Approach

Lorenzo Boldrini

CREATES Research Paper 2015-40

Department of Economics and Business Economics
Aarhus University
Fuglesangs Allé 4
DK-8210 Aarhus V
Denmark

Email: oekonomi@au.dk
Tel: +45 8716 5515

Forecasting the Global Mean Sea Level, a Continuous-Time State-Space Approach

Lorenzo Boldrini *

August 27, 2015

Abstract

In this paper we propose a continuous-time, Gaussian, linear, state-space system to model the relation between global mean sea level (GMSL) and the global mean temperature (GMT), with the aim of making long-term projections for the GMSL. We provide a justification for the model specification based on popular semi-empirical methods present in the literature and on zero-dimensional energy balance models. We show that some of the models developed in the literature on semi-empirical models can be analysed within this framework. We use the sea-level data reconstruction developed in Church and White (2011) and the temperature reconstruction from Hansen et al. (2010). We compare the forecasting performance of the proposed specification to the procedures developed in Rahmstorf (2007b) and Vermeer and Rahmstorf (2009). Finally, we compute projections for the sea-level rise conditional on the 21st century SRES temperature scenarios of the IPCC fourth assessment report. Furthermore, we propose a bootstrap procedure to compute confidence intervals for the projections, based on the method introduced in Rodriguez and Ruiz (2009).

Keywords: energy balance model, semi-empirical model, state-space system, Kalman filter, forecasting, temperature, sea level, bootstrap.
JEL classification: C32.

*Aarhus University, Department of Economics and Business Economics, CREATES - Center for Research in Econometric Analysis of Time Series, Fuglesangs Allé 4, 8210 Aarhus V, Denmark. Email: lboldrini@econ.au.dk. The author acknowledges support from CREATES - Center for Research in Econometric Analysis of Time Series (DNRF78), funded by the Danish National Research Foundation.

1 Introduction

Climate changes, the increase in the global temperature and sea level are long-standing topics. Monitoring and predicting the rise in the sea level is of great importance due to its close relation with global climate changes and the socio-economic effects it entails. In particular, the sea-level rise has direct consequences for populations living near the current mean sea level, Anthoff et al. (2006), Anthoff et al. (2010), Arnell et al. (2005), Sugiyama et al. (2008). Physical and statistical models are needed to measure the rate of change of the sea level and understand its relation to anthropogenic and natural causes.

In this paper we propose a statistical framework to model the relation between the global mean sea level (GMSL) and the global mean temperature (GMT), with the aim of making long-term projections for the GMSL. The model belongs to the class of semi-empirical models. We provide a justification for the model specification based on popular semi-empirical methods present in the literature and on zero-dimensional energy balance models. We show that some of the semi-empirical models developed in the literature to study the relation between sea-level rise and temperature can be analysed within this framework.

To date, there are two methods of estimating the sea-level rise as a function of climate forcing. The conventional approach, used by the Intergovernmental Panel on Climate Change (IPCC) climate assessments, is to use process-based models to estimate contributions from the sea-level components and then sum them to obtain an estimate of the sea-level increase, see for instance Meehl et al. (2007), Meehl et al. (2007), Pardaens et al. (2011), Solomon et al. (2009). Variations in the sea level originate from steric, eustatic, and non-climate changes. By steric, we mean sea-level variations due to ocean volume changes, resulting from temperature (thermosteric) and salinity (halosteric) variations. By eustatic, we mean variations in the mass of the oceans as a result of water exchanges between the oceans and other surface reservoirs (ice sheets, glaciers, land water reservoirs, and the atmosphere)[1]. By non-climate causes we mean variations in the quantity of water in the oceans due to human impact, such as the building of dams and the extraction of groundwater. However, the theoretical understanding of the different contributors is incomplete, as IPCC models under-predict rates of sea-level increase.

The alternative way of making projections of the sea level is the class of semi-empirical models. These models analyse statistical relationships using physically plausible models of reduced complexity in which the sea-level rate of change depends on the global temperature. The main idea behind semi-empirical models is that the steric and eustatic contributors to the sea level (the major ones) respond to changes in the global temperature. The first semi-empirical model was proposed by Gornitz et al. (1982) who specify a linear relation between sea level and temperature. Some more recent models where developed by specifying a differential equation, relating the sea level to temperature or other climate forcing. Representative examples are Rahmstorf (2007b), Vermeer and Rahmstorf (2009), Grinsted et al. (2010), Kemp et al. (2011), Jevrejeva et al. (2009), Jevrejeva et al. (2010), Jevrejeva et al. (2012b), Jevrejeva et al. (2012a).

All semi-empirical models project higher sea-level rise, for the 21st century, that the last generation of process-based models, summarized in the IPCC Fourth Assessment Report, see for instance Moore et al. (2013), Cazenave and Nerem (2004), Munk (2002), and

[1] In this paper we adopt the same definitions of steric and eustatic used in Cazenave and Nerem (2004).

Rahmstorf (2007b). A comprehensive survey on the different process-based and semi-empirical models can be found in Moore et al. (2013).

We propose a state-space approach to forecast the global mean sea level, conditional on the global mean temperature. State-space systems allow to address the problems of smoothing, detrending, and parameter estimation in a unique framework. We consider in particular continuous-time, linear, Gaussian state-space systems of the type described in Bergstrom (1997). More specifically, the state vector follows a multivariate, Gaussian, OrnsteinUhlenbeck process. The discretised system preserves its linearity and Kalman filtering techniques apply. In particular, the Kalman filter is used for two tasks: the first one is to compute the likelihood function of the state-space system, needed for parameter estimation, and the second one is to make forecasts of the sea level, conditional on the temperature.

The statistical framework of state-space systems allows to distinguish between measurement noise and model uncertainty, through the measurement and state equations, respectively. Furthermore, in this setup it is possible to consider different levels of measurement noise for different points in time. In fact, the reconstructions of the sea level, in particular, are typically very noisy and the measurements uncertainty reflects, for instance, the changes in the measurement instruments throughout the decades, as well as the changes in the data sources. In this study we use the sea-level reconstruction from Church and White (2011), who also provide an estimate of the uncertainty of their sea-level estimates. In the state-space approach these uncertainties (measured as standard deviations) are directly used to parameterise the time-varying variances of the measurement errors of the sea-level time series. Temperature data are taken from Hansen et al. (2010). Both sea level and temperature data correspond to monthly reconstructions.

We provide a justification for the model specification based on popular semi-empirical methods present in the literature and on zero-dimensional energy balance models. In more detail, we specified the system dynamics of sea level and temperature as well as the functional form linking these variables, consistently with the ones suggested by the existing literature. We show that some of the semi-empirical models developed in the literature to study the relation between sea level and temperature, can be analysed within this framework.

Semi-empirical models are usually specified as differential equations, as in Rahmstorf (2007b), Vermeer and Rahmstorf (2009), Grinsted et al. (2010), Kemp et al. (2011), Jevrejeva et al. (2009), Jevrejeva et al. (2010), Jevrejeva et al. (2012b), and Jevrejeva et al. (2012a). By specifying the state-space system in continuous time and then deriving the exact discrete-time system, we can make inference on the structural parameters driving the continuous-time process. A similar approach was used in Pretis (2015) (forthcoming), in which the author shows the equivalence of a two-component energy balance model to a cointegrated system. He then shows the exact mapping between the continuous-time system to the discrete-time one, that amounts to a cointegrated vector autoregressive system.

In the literature on semi-empirical models, state-space system representations and the Kalman filter are often used with the aim of assimilating noisy measurements from different sources[2]. Such studies are for instance, Miller and Cane (1989) and Chan et al.

[2]In this context, assimilation usually refers to the filtering of a variable, measured at a specific point in time and geographic location, by taking into account information from measurements taken at neigh-

(1996) who use the Kalman filter with an underlying physical model to assimilate average sea-level anomalies from tide gauge measurements and Cane et al. (1996) and Hay et al. (2013).

The paper is organised as follows: in Section 2, we explain the statistical framework and introduce the model specification, showing how it relates to some important models in the literature; in Section 3, we describe the dataset; in Section 4, we illustrate the forecasting procedures; in Section 5, we provide some details on the computational aspects of the analysis; in Section 6, we present results; finally, Section 7 concludes.

2 Model specification

2.1 Energy balance models and temperature dynamics

In this section we present the foundations for the temperature process used in the state-space model proposed in Section 2.3. This section draws heavily on North et al. (1981) and Imkeller (2001) and we refer the reader to these papers for more details. The starting model, for the temperature, belongs to the class of zero-dimensional energy balance models (EBMs), detailed in North et al. (1981), and whose review is based on the models introduced in Budyko (1968), Budyko (1969), Budyko (1972), and Sellers (1969). These models are based on thermodynamic concepts and global radiative heat balance, for the Earth system. This type of models describe the global temperature process as (possibly stochastic) univariate, differential equations. In particular, the change in the Planet's global temperature at time t is seen as a function of the difference between the incoming and outgoing radiation.

The incoming (absorbed) radiation R_{in} is caused by solar irradiance (i.e. the sunlight reaching the Earth) and is affected by the reflectivity of the Planet. The incoming radiation is then a function of the solar constant[3] σ_0, the albedo coefficient[4] α, and the radius R of the Earth, in particular: $R_{in} = \sigma_0(1-\alpha)\pi R^2$. The outgoing radiation R_{out} is assumed, for simplicity, to be black-body[5] radiation, obeying the Stefan-Boltzmann law[6]. It is then a function of the absolute temperature T of the Planet and its radius R, in particular: $R_{out} = 4\pi R^2 k_{SB} T^4$.

The analysis of zero-dimensional EBMs begins with the concept of global radiative heat balance. In radiative equilibrium the rate at which solar radiation is absorbed by the Planet matches the rate at which infrared radiation is emitted by it. The condition

bouring locations at the same point in time. If the filtered variables are output from the Kalman filter, the contribution of variable j to the estimate of variable i is given by element (i, j) of the Kalman gain matrix.

[3]The solar constant is a measure of the mean solar electromagnetic radiation per unit area that would be incident on a plane perpendicular to the sun rays.

[4]The term albedo, Latin for white, describes the average reflection coefficient of an object. The greenhouse effect, for instance, can lower the albedo of the Earth, and cause global warming.

[5]A black body is an idealized physical object that absorbs all incident electromagnetic radiation. The total energy per unit of time, per unit of surface area, radiated by a black body depends solely on its absolute temperature and obeys the Stefan-Boltzman law.

[6]The Stefan-Boltzmann law describes the power radiated from a black body in terms of its thermodynamic temperature. The thermodynamic temperature (absolute temperature) is commonly expressed in Kelvin $[K]$, where $0[K] = -273.15[^\circ\text{C}]$ corresponds to the lowest achievable temperature, according to the third principle of thermodynamics.

of radiative equilibrium is given by

$$\overbrace{4\pi R^2 k_{SB} T^4}^{R_{out}} = \overbrace{\sigma_0(1-\alpha)\pi R^2}^{R_{in}}, \tag{1}$$

where T is the effective radiating temperature of the Planet, and $k_{SB} = 0.56687 \cdot 10^{-7}[Wm^{-2}K^4]$, is the Stefan-Boltzmann constant. Note that both sides of equation (1) are expressed in units of power, in particular in Watts $[W]$. When the incoming radiation does not match the outgoing radiation, the temperature of the Planet changes in order to compensate the disequilibrium. The time-evolution of the temperature can then be modelled with the following zero-dimensional EBM:

$$\begin{aligned} C\frac{dT(t)}{dt} &= R_{in} - R_{out} \\ &= \sigma_0(1-\alpha)\pi R^2 - 4\pi R^2 k_{SB} T^4(t), \end{aligned} \tag{2}$$

where C, that has units of $\left[\frac{W \cdot s}{K}\right] = \left[\frac{J}{K}\right]$, represents global thermal inertia and regulates the speed of the temperature response. With $T(t)$ we make explicit the dependence of temperature on time. Equation (2) can be written as

$$C\frac{dT(t)}{dt} = Q\hat{\alpha} - \gamma T^4(t), \tag{3}$$

where Q is a constant proportional to σ_0, γ is a constant proportional to k_{SB}, and $\hat{\alpha} = (1-\alpha)$ is the co-albedo. Note that equation (3) allows to relax the black-body assumption. In fact, for a so called grey body[7] we have that the emissive power, per unit surface area is $I = \varepsilon k_{SB} T^4$, with $\varepsilon < 1$.

Equation (3) is purely deterministic. To allow for random forcing, stochastic EBM have been introduced, see for instance Fraedrich (1978) and Hasselmann (1976). A stochastic EBM can be written in the following way:

$$C\frac{dT(t)}{dt} = Q\hat{\alpha} - \gamma T^4(t) + \dot{W}(t), \tag{4}$$

where $\dot{W}(t)$ is a white noise random forcing[8].

Depending on the time scale under examination, the solar constant funtion Q can be allowed to be time-varying. For instance, the Milankovich cycle responsible for the glaciations, i.e. a cyclical mutation in the eccentricity of the Earth orbit due to the gravitational pull of other planets, has a period of approximately 10^5 years and can be expressed as $Q(t) = Q_0 + sin(\omega t)$ with $\omega = 10^{-5}[1/year]$, see Imkeller (2001). Similarly, the co-albedo $\hat{\alpha}$ can be assumed to be time-varying and, in particular, to depend on the global temperature, i.e. $\hat{\alpha}(T(t))$. This is motivated, among other reasons, by the ice-cap feedback. That is, the albedo of the Planet changes with the temperature as a result of the shrinking or spreading of ice sheets on the Earth's surface, that depends on the global

[7] A body that does not absorb all incident radiation.

[8] The white noise process is defined as $E[\dot{W}(t)]$ and $E[\dot{W}(t)\dot{W}(t')] = q^2\delta(t-t')$ where $\delta(t-t')$ is a Dirac delta, and q is a constant, see also Nicolis (1982).

temperature.

Taking into consideration these arguments, equation (4) can be written in the form

$$\begin{aligned} C\frac{dT(t)}{dt} &= R_{in} - R_{out} + \dot{W}(t) \\ &= Q(t)\hat{\alpha}(T(t)) - \gamma T^4(t) + \dot{W}(t). \end{aligned} \tag{5}$$

Different specifications for R_{in} and R_{out} have been suggested in the literature. Budyko (1969), for instance, suggested that the infrared radiation to space, R_{out}, can be represented as a linear function of the surface temperature T, that is:

$$4\pi R^2 \sigma T^4(t) \cong 4\pi R^2 \sigma(\delta_1 + \delta_2 T(t)), \tag{6}$$

where δ_1, and δ_2 are constants, taking into account factors such as average cloudiness, the effects of infrared absorbing gases, and the variability of water vapor. Sellers (1969) suggested taking a linear approximation also of the albedo, or similarly, of the co-albedo:

$$\hat{\alpha}(T(t)) = \beta_1 + \beta_2 T(t), \tag{7}$$

where β_1 and β_2 are constants.

We now show that some important special cases of model (5) can be written in the form

$$dT(t) = \left\{b^T + \kappa^T \mu^T(t) + a^{TS} S(t) + a^{TT} T(t)\right\} dt + d\eta^T(t), \tag{8}$$

where b^T, a^{TS}, a^{TT}, and κ^T are constants, $\mu^T(t)$ is a time-varying process, $S(t)$ is the sea-level process, and $\eta^T(t)$ is a scaled Brownian motion with $E[d\eta^T(t)d\eta^T(t)] = \Sigma^{TT}dt$. In particular, equation (8) is an exact representation of model (5) for these specifications:

I. for a time-invariant solar constant Q, a constant co-albedo $\hat{\alpha}$, and taking a linear approximation to $R_{out} = \gamma T^4(t) \cong \delta_1 + \delta_2 T(t)$, we obtain the following relation between the componets of equation (5) and the ones of equation (8):

$$b^T = \frac{1}{C}(Q\hat{\alpha} - \delta_1), \quad \kappa^T \mu^T(t) = 0, \quad a^{TS} = 0, \quad a^{TT} = -\frac{1}{C}\delta_2, \quad d\eta^T(t) \neq 0; \tag{9}$$

II. for a time-varying solar constant $Q(t)$, a constant co-albedo $\hat{\alpha}$, and taking a linear approximation to $R_{out} = \gamma T^4(t) \cong \delta_1 + \delta_2 T(t)$, we obtain:

$$b^T = -\frac{1}{C}\delta_1, \quad \kappa^T \mu^T(t) = \frac{1}{C}Q(t)\hat{\alpha}, \quad a^{TS} = 0, \quad a^{TT} = -\frac{1}{C}\delta_2, \quad d\eta^T(t) \neq 0; \tag{10}$$

III. for a time-varying solar constant $Q(t)$, a time varying co-albedo $\hat{\alpha}(t)$, and a linear approximation to $R_{out} = \gamma T^4(t) \cong \delta_1 + \delta_2 T(t)$, we have:

$$b^T = -\frac{1}{C}\delta_1, \quad \kappa^T \mu^T(t) = \frac{1}{C}Q(t)\hat{\alpha}(t), \quad a^{TS} = 0, \quad a^{TT} = -\frac{1}{C}\delta_2, \quad d\eta^T(t) \neq 0; \tag{11}$$

IV. for a time-invariant solar constant Q, a time varying co-albedo, assuming dependence on the temperature of the co-albedo $\hat{\alpha}(T(t))$ and linearity in the temperature $\hat{\alpha}(T(t)) = \beta_1 + \beta_2 T(t)$, and taking a linear approximation $R_{out} = \gamma T^4(t) \cong \delta_1 + \delta_2 T(t)$, we obtain:

$$b^T = \frac{1}{C}(Q\beta_1 - \delta_1), \quad \kappa^T \mu^T(t) = 0, a^{TS} = 0, \quad a^{TT} = \frac{1}{C}(Q\beta_2 - \delta_2), \quad d\eta^T(t) \neq 0. \tag{12}$$

The time-varying component $\kappa^T \mu^T(t)$ controls for changes in the albedo and/or solar constant coefficients. That is, it accounts among other things, for the effects of greenhouse gases and other phenomena that change the radiation-absorbing properties of the Planet.

2.2 Semi-empirical models and sea-level dynamics

Some of the most representative semi-empirical models in the literature are here briefly presented. Throughout this section we denote with t time, $S(t)$ the global mean sea level, and with $T(t)$ the global mean temperature. Parameters are indicated with lower case letters. We consider the following five models:

I. Gornitz et al. (1982) suggest the following link between sea level and temperature:

$$S^*(t) \quad = \quad aT^* \left(t - t_0\right) + b, \tag{13}$$

where S^* and T^* are the 5-year averages of the global sea level and temperature, respectively. The parameters a and b are estimated by least-squares linear regression and the time lag t_0 is chosen to minimize the variance between (13) and the sea-level curve.

II. Rahmstorf (2007b) suggests the following differential equation relating sea level to temperature:

$$\frac{dS(t)}{dt} \quad = \quad r\left(T(t) - T_0\right), \tag{14}$$

where r is a parameter to be estimated. The sea-level rise above the previous equilibrium state can be computed as

$$S(t) = r \int_{t_0}^{t} \left(T(s) - T_0\right) ds. \tag{15}$$

The statistical analysis in Rahmstorf (2007b) is comprised of several steps. First, the GMSL and GMT series are processed to obtain annual means. Second, a singular spectrum analysis filter, with a 15-year smoothing period, is applied to the series of yearly averages. Third, data is divided into 5 years bins, in which the average is taken. Lastly, the resulting sea-level series in first differences is regressed on the resulting temperature in levels (with optional detrending of both series before the regression). The data they use are the global mean sea level from Church and White (2006) and the global temperature anomalies data from GISTemp, Hansen et al. (2001). See Holgate et al. (2007) and Rahmstorf (2007a) for comments on the statistical procedure.

III. Vermeer and Rahmstorf (2009) suggest the following extension of the previous model:

$$\frac{dS(t)}{dt} = v_1 \left(T(t) - T_0\right) + v_2 \frac{dT(t)}{dt}. \tag{16}$$

In this model the authors add the term $v_2 \frac{dT(t)}{dt}$ to the Rahmstorf (2007b) model, corresponding to an "instantaneous" sea-level response. The statistical methodology is similar to the one in Rahmstorf (2007b) and a thorough description of it can be found in the online appendix to their paper.

IV. Kemp et al. (2011) propose the following model:

$$\begin{aligned} \frac{dS(t)}{dt} &= k_1 \left(T(t) - T_{0,0}\right) + k_2 \left(T(t) - T_0(t)\right) + k_3 \frac{dT(t)}{dt}, \\ \frac{dT_0(t)}{dt} &= \frac{T(t) - T_0(t)}{\tau}. \end{aligned} \tag{17}$$

The first term captures a slow response compared to the time scale of interest, the second one captures intermediate time scales, where an initial linear rise gradually saturates with time scale τ as the base temperature T_0 catches up with $T(t)$. In Rahmstorf (2007b), equation (14), T_0 was assumed to be constant. The third term is the immediate response term introduced by Vermeer and Rahmstorf (2009).

V. Grinsted et al. (2010) propose the following model:

$$\begin{aligned} S_{eq} &= g_1 T + g_2, \\ \frac{dS(t)}{dt} &= \frac{S_{eq} - S(t)}{\tau}, \end{aligned} \tag{18}$$

where S_{eq} is the equilibrium sea level, for a given temperature. They assume a linear approximation of the relation between sea level and temperature, due to the closeness of the current sea level to the equilibrium in this climate period (late Holocene-Anthropocene) and for small changes in the sea level. Equation (18) can be integrated to give the sea level S over time, using the history of the temperature T and knowledge of the initial sea level at the start of integration S_0. They impose constraints on the model, suggested by reasonable physical assumptions.

We here show how some of the different model specifications for the relation between sea level and temperature can be seen as special cases of the following stochastic differential equation

$$dS(t) = \left\{b^S + \kappa^S \mu^S(t) + a^{SS} S(t) + a^{ST} T(t)\right\} dt + d\eta^S(t), \tag{19}$$

where b^S, κ^S, a^{SS}, and a^{ST} are parameters, $\mu^S(t)$ is a time-dependent process, and $\eta^S(t)$ is a scaled Brownian motion with $E[d\eta^S(t) d\eta^S(t)] = \Sigma^{SS} dt$. In particular, models II and V can be written as particular cases of model (19) if some restrictions are imposed on its components:

II. for the Rahmstorf (2007b) specification we have the following relation between the components of equation (19) and equation (14):

$$b^S = -rT_0, \qquad \kappa^S \mu^S(t) = 0, \qquad a^{SS} = 0, \qquad a^{ST} = r, \qquad d\eta^S(t) = 0; \tag{20}$$

V. for the Grinsted et al. (2010) specification, the relation between the components of equation (19) and (18) are:

$$b^S = \frac{1}{\tau} g_2, \qquad \kappa^S \mu^S(t) = 0, \qquad a^{SS} = -\frac{1}{\tau}, \qquad a^{ST} = \frac{1}{\tau} g_1, \qquad d\eta^S(t) = 0. \tag{21}$$

Note that in models II and V the component $\kappa^S \mu^S(t)$ is zero. This reflects the fact that in both papers the series of temperature and sea level are detrended before the parameter estimation. Instead, we prefer to model the trend component jointly with the temperature and sea-level dynamics.

2.3 State-space system

Combining the temperature and sea-level dynamics, equations (8) and (19), we obtain the following multivariate process

$$d \begin{bmatrix} S(t) \\ T(t) \end{bmatrix} = \mathbf{b} dt + \begin{bmatrix} a^{SS} & a^{ST} \\ a^{TS} & a^{TT} \end{bmatrix} \begin{bmatrix} S(t) \\ T(t) \end{bmatrix} dt + \begin{bmatrix} \kappa^S & 0 \\ 0 & \kappa^T \end{bmatrix} \begin{bmatrix} \mu^S(t) \\ \mu^T(t) \end{bmatrix} dt + d\boldsymbol{\eta}(t), \tag{22}$$

where $\mathbf{b} = [b^S : b^T]'$, $\boldsymbol{\mu}(t) = [\mu^S(t) : \mu^T(t)]'$ is the trend component, and $d\boldsymbol{\eta}(t) = [d\eta^S(t) : d\eta^T(t)]'$ where $\boldsymbol{\eta}(t)$ is a scaled, 2-dimensional, Brownian motion with $E[d\boldsymbol{\eta}(t) d\boldsymbol{\eta}(t)'] = \boldsymbol{\Sigma} dt$ and

$$\boldsymbol{\Sigma} = \begin{bmatrix} \Sigma^{SS} & \Sigma^{ST} \\ \Sigma^{TS} & \Sigma^{TT} \end{bmatrix}, \tag{23}$$

a positive semidefinite covariance matrix.
We consider two parametric forms for the trend component $\boldsymbol{\mu}(t)$, namely a linear and a quadratic trend:

(i) linear trend component,

$$d\boldsymbol{\mu}(t) = \boldsymbol{\lambda}_l dt, \tag{24}$$

where $\boldsymbol{\lambda}_l = [\lambda_l^S : \lambda_l^T]$ are parameters to be estimated;

(ii) quadratic trend component,

$$\begin{aligned} d\boldsymbol{\mu}(t) &= \boldsymbol{\lambda}(t) dt, \\ d\boldsymbol{\lambda}(t) &= \boldsymbol{\nu}_q dt, \end{aligned} \tag{25}$$

where $\boldsymbol{\lambda}(t) = [\lambda^S(t) : \lambda^T(t)]'$ is a 2-dimensional process and $\boldsymbol{\nu}_q = [\nu_q^S : \nu_q^T]'$ are parameters to be estimated.

The choice of the trend components was driven by the forecast performance of the models, according to the forecasting exercise detailed in Section 4.1.

2.3.1 State equation

We now show how to obtain the exact discrete representation of the continuous-time state-space system (22) with linear trend (24) (the derivation for the model with the quadratic trend (25) is analogous). The system of equations (22)-(24) can be written in compact form, delivering the followin Gaussian, Ornstein-Uhlenbeck (OU) process:

$$d\boldsymbol{\alpha}(t) \;=\; \mathbf{c}dt + \mathbf{A}\boldsymbol{\alpha}(t)dt + d\boldsymbol{\xi}(t), \tag{26}$$

where $\boldsymbol{\alpha}(t) = [S(t), T(t), \mu^S(t), \mu^T(t)]'$, $\mu^S(t)$ and $\mu^T(t)$ indicate the trends for the sea-level and the temperature, respectively, $d\boldsymbol{\xi}(t) = [d\boldsymbol{\eta}(t)' : \mathbf{0}']'$, $\mathbf{c} = [\mathbf{b}' : \boldsymbol{\lambda}_l']' = [\mathbf{0}' : \boldsymbol{\lambda}_l']'$, and the autoregressive matrix has the form

$$\mathbf{A} \;=\; \begin{bmatrix} a^{SS} & a^{ST} & 1 & 0 \\ a^{TS} & a^{TT} & 0 & 1 \\ 0 & 0 & 0 & 0 \\ 0 & 0 & 0 & 0 \end{bmatrix}, \tag{27}$$

where we constrain the two parameters $\kappa^S = \kappa^T = 1$, as suggested in Bergstrom (1997), in order to avoid identification issues. We set the intercept $\mathbf{b} = \mathbf{0}$ because of the presence of trend component. The exact discrete state-space representation can be recovered from the continuous-time equations following, for instance, Bergstrom (1997). The solution of the OU process (22) is

$$\boldsymbol{\alpha}(t) \;=\; e^{t\mathbf{A}}\boldsymbol{\alpha}(0) + \int_0^t e^{\mathbf{A}(t-s)}\mathbf{c}ds + \int_0^t e^{\mathbf{A}(t-s)}d\boldsymbol{\xi}(s), \tag{28}$$

where $\boldsymbol{\alpha}(0)$ is the initial value of the system. Note that the solution (28) always exists.

Denote with $\tau = 1, \ldots, n$, $n \in \mathbb{N}$, the time instances at which the sea-level and the temperature processes are sampled (measured), i.e. $\boldsymbol{\alpha}(t = \tau) = \boldsymbol{\alpha}_\tau$. The relationship between the state vector at time τ and time $\tau + 1$ derives from equation (28) and is given by

$$\boldsymbol{\alpha}_{\tau+1} \;=\; e^{\mathbf{A}}\boldsymbol{\alpha}_\tau + \int_\tau^{\tau+1} e^{\mathbf{A}(\tau+1-s)}\mathbf{c}ds + \int_\tau^{\tau+1} e^{\mathbf{A}(\tau+1-s)}d\boldsymbol{\xi}(s). \tag{29}$$

Equation (29) corresponds to a Gaussian, vector autoregressive process of this form

$$\boldsymbol{\alpha}_{\tau+1} \;=\; \mathbf{c}^* + \mathbf{A}^*\boldsymbol{\alpha}_\tau + \boldsymbol{\xi}_\tau, \tag{30}$$

with $\boldsymbol{\xi}_\tau \sim N(\mathbf{0}, \boldsymbol{\Sigma}^*)$, where

$$\begin{aligned} \mathbf{c}^* &= \int_0^1 e^{\mathbf{A}(1-s)}\mathbf{c}ds, \\ \mathbf{A}^* &= e^{\mathbf{A}}, \\ \boldsymbol{\Sigma}^* &= \int_0^1 e^{\mathbf{A}(1-s)}\boldsymbol{\Sigma}e^{\mathbf{A}'(1-s)}ds. \end{aligned} \tag{31}$$

The constants a^{SS}, a^{ST}, a^{TS}, a^{TT}, $\boldsymbol{\lambda}$, and $\boldsymbol{\Sigma}$ are parameters to be estimated.

2.3.2 Measurement equation

The global mean sea level and the global mean temperature can be seen as stock variables, sampled at time instances τ and subject to measurement error, see for instance Harvey and Stock (1993). Let S_τ^r and T_τ^r be the reconstructed (or measured) sea-level and temperature processes, respectively, and S_τ and T_τ the *true* (unobserved), latent ones. The measurement equation for system (30) is thus:

$$\begin{bmatrix} S_\tau^r \\ T_\tau^r \end{bmatrix} = \begin{bmatrix} S_\tau \\ T_\tau \end{bmatrix} + \begin{bmatrix} \epsilon_\tau^S \\ \epsilon_\tau^T \end{bmatrix}, \tag{32}$$

where $\boldsymbol{\epsilon}_\tau = [\epsilon_\tau^S : \epsilon_\tau^T]' \sim N(\mathbf{0}, \mathbf{H}_\tau)$ is a bivariate random vector of independent measurement errors. Note that the variance-covariance matrix is allowed to vary through time, in particular

$$\mathbf{H}_\tau = \begin{bmatrix} \sigma_\tau^{2,S} & 0 \\ 0 & \sigma^{2,T} \end{bmatrix}. \tag{33}$$

The variance of the measurement error for the sea level $\sigma_\tau^{2,S}$, is allowed to change in time. In particular, in this work we use the sea-level reconstruction from Church and White (2011). In their analysis, the authors provide uncertainty estimates of the sea-level reconstruction at each point in time. The change in the uncertainty of the reconstructed sea-level series reflects the change in time of the measurement instruments, as well as the change in the data sources. Note that in this context, the magnitude of the observation error variances controls the smoothness of the filtered series of sea level and temperature. The parameter $\sigma^{2,T}$ is estimated together with the other system parameters, whereas the sequence $\{\sigma_\tau^{2,S}\}_{\tau=1:n}$ is fixed and corresponds to the uncertainty values reported in Church and White (2011).

Combining equations (30) with (32) we obtain a linear, Gaussian, state-space system (see for instance Brockwell and Davis (2009) and Durbin and Koopman (2012)):

$$\begin{aligned} \begin{bmatrix} S_\tau^r \\ T_\tau^r \end{bmatrix} &= \begin{bmatrix} 1 & 0 & 0 & 0 \\ 0 & 1 & 0 & 0 \end{bmatrix} \begin{bmatrix} S_\tau \\ T_\tau \\ \mu_\tau^S \\ \mu_\tau^T \end{bmatrix} + \boldsymbol{\epsilon}_\tau, & \boldsymbol{\epsilon}_\tau &\sim N(\mathbf{0}, \mathbf{H}_\tau), \\ \begin{bmatrix} S_{\tau+1} \\ T_{\tau+1} \\ \mu_{\tau+1}^S \\ \mu_{\tau+1}^T \end{bmatrix} &= \mathbf{c}^* + \mathbf{A}^* \begin{bmatrix} S_\tau \\ T_\tau \\ \mu_\tau^S \\ \mu_\tau^T \end{bmatrix} + \boldsymbol{\xi}_\tau, & \boldsymbol{\xi}_\tau &\sim N(\mathbf{0}, \boldsymbol{\Sigma}^*). \end{aligned} \tag{34}$$

System (34) is linear in the state variables and Kalman filtering/smoothing techniques apply, allowing to estimate the system parameters by maximum likelihood, see for instance Durbin and Koopman (2012).

In the semi-empirical literature, dynamic models of sea level and temperature are usually formulated in continuous time. A clear mapping between a multivariate, Gaussian, Ornstein-Uhlenbeck process and its discrete-time analogue allows to make inference on the parameters of the original process, introducing no bias due to discretizations. A convenient aspect of specifying the model in state-space form is that measurement noise

and trends can be modelled in a joint framework. In this way the problem of smoothing, detrending, and parameter inference can be handled in a unified framework.

The dimensional analysis for the continuous-time and discrete-time systems is provided in Appendix C.

3 Data

- **Temperatures**. The temperature data are taken from the GISS dataset, Combined Land-Surface Air and Sea-Surface Water Temperature Anomalies (Land-Ocean Temperature Index, LOTI). The values are temperature anomalies, i.e. deviations from the corresponding 1951-1980 means, Hansen et al. (2010)[9]. The time series we use is composed of mean global monthly values. The values of the original series are in centi-degrees Celsius ($[\text{c}^\circ\text{C}] = 10^{-2}[^\circ\text{C}]$).

- **Sea level**. The sea-level data is from Church and White (2011)[10]. The authors also provide uncertainty estimates for each measurement. They estimate the rise in global average sea level from satellite altimeter data for 1993-2009 and from coastal and island sea-level measurements from 1880 to 2009. The measurements of the original series are in millimetres [mm].

In our analysis we use monthly observations ranging from January 1880 to December 2009, range in which the two series overlap, for a sample size equal to 1560.

- **IPCC temperature scenarios**. These series correspond to reconstructed and simulated annual temperatures, from 1900 to 2099 from the 2007 IPCC Fourth Assessment Report, SRES scenarios. In particular, we use the A1b, A2, B1, and commit groups of temperature scenarios[11]. The 4 groups correspond to different "storylines"[12]. The storylines "describe the relationships between the forces driving greenhouse gas and aerosol emissions and their evolution during the 21st century for large world regions and globally. Each storyline represents different demographic, social, economic, technological, and environmental developments that diverge in increasingly irreversible ways." (Carter (2007, page 9)). Each group has a different number of scenarios and in total there are 75 scenarios. The 4 scenarios groups can be described in the following way:

  (i) **A1b group**. This group belongs to the A1 storyline and scenario family, that is "a future World of very rapid economic growth, global population that peaks in mid-century and declines thereafter, and rapid introduction of new and more efficient technologies." (Carter (2007, page 9)) in which an intermediate level of emissions has been assumed. There are 21 scenarios belonging to this group.

  (ii) **A2 group**. "A very heterogeneous World with continuously increasing global population and regionally oriented economic growth that is more fragmented

[9]Data can be downloaded from `http://data.giss.nasa.gov/gistemp/`.

[10]Data can be downloaded from `http://www.cmar.csiro.au/sealevel/sl_data_cmar.html`.

[11]Data can be downloaded from `http://www.ipcc-data.org/sim/gcm_global/index.html`.

[12]For a precise description of the storylines and scenarios see Carter (2007), `http://www.ipcc-data.org/guidelines/TGICA_guidance_sdciaa_v2_final.pdf`.

and slower than in other storylines." (Carter (2007, page 9)). There are 17 scenarios belonging to this group.

(iii) **B1 group**. "A convergent World with the same global population as in the A1 storyline but with rapid changes in economic structures toward a service and information economy, with reductions in materials intensity, and the introduction of clean and resource-efficient technologies." (Carter (2007, page 9)). There are 21 scenarios belonging to this group.

(iv) **commit group**. In this group of scenarios, the World's countries commit to lower greenhouse gases emissions. There are 16 scenarios belonging to this group.

The A1b and A2 groups reflect scenarios with an acceleration in temperature growth (high temperature increase); the B1 group reflects scenarios of constant temperature growth (medium temperature increase); the commit group reflects scenarios of very low temperature growth (low temperature increase). The measurements of the original series are in degrees Celsius [°C].

4 Forecasting

4.1 Model comparison

To assess the forecasting power of the state-space models proposed in Section 2.3, we carry out the following forecasting exercise. Let n denote the complete sample size (i.e. $n = 1560$, corresponding to monthly observations ranging from January 1880 to December 2009), $n^* < n$ the size of the estimation sample, h the forecast horizon, $f = n - n^*$ the number of forecasts for a given estimation sample size. For all forecasting methods, the setup of the exercise is the following:

1. estimate the system parameters using observations of sea level and temperature from time $t = 1$ up to $t = n^*$;

2. compute forecasts using temperature observations from time $t = n^* + 1$ to $t = n$.

In particular, for the state-space system (34) (and for the model with quadratic trend) the steps to construct the forecasts are the following :

(i) estimate the system parameters by maximum likelihood, using observations of sea level and temperature from time $t = 1$ up to $t = n^*$ (the likelihood function is delivered by the Kalman filter, see for instance Durbin and Koopman (2012));

(ii) run the Kalman filter, using the estimated parameters, on the dataset composed of observations of the sea level from time $t = 1$ to $t = n^*$ and observations of the temperature from $t = 1$ to $t = n$.

(iii) the forecasts of the sea level are then the filtered values $\hat{S}_{n^*+h}$ with $h = 1, \ldots, f$.

Observations of the sea level, from time $t = n^* + 1$ to $t = n$, are treated as missing values, see Durbin and Koopman (2012) for more details on how to modify the filter in

case of missing observations. Note that for a linear state-space system the Kalman filter delivers the best linear predictions of the state vector, conditionally on the observations. Moreover, if the innovations are Gaussian, the filtered states coincide with conditional expectations, for more details on the optimality properties of the Kalman filter see Brockwell and Davis (2009).

We select two benchmark forecasting methods to which we compare our specifications. In particular, we compare our model to the procedures developed in Rahmstorf (2007b) and Vermeer and Rahmstorf (2009). The choice of these benchmarks reflects their popularity in the literature and the replicability of the results in the papers due to the availability of source codes.

4.1.1 Rahmstorf (2007b) procedure

The first competing method is the one used in Rahmstorf (2007b). The model is based on equations (14)-(15). The procedure can be summarized as follows:

(i) the sea-level and temperature series, from time $t = 1$ up to $t = n^*$, are smoothed using singular spectrum analysis and embedding dimension equal to $n_{ed} = 180$ months, corresponding to 15 years ($15 \times 12 = 180$), as used in their paper;

(ii) first differences of the smoothed sea-level series are then taken;

(iii) the smoothed series (temperature and first differences of the sea level) are then divided into $n_{bin} = 60$ months bins, corresponding to 5 years ($5 \times 12 = 60$), as used in the paper, and in each bin the average is taken;

(iv) the time series of bin-averages are then detrended (fitting a linear trend);

(v) the bin-averages of sea level in first differences is then regressed onto the bin-averages of the temperature in levels;

(vi) the estimated regression coefficients are then used to compute the values of the sea level in first differences from the out-of-sample (smoothed) temperatures (note that the information set used comprises the sea-level observations from time $t = 1$ to $t = n^*$, and observations of the temperature from $t = 1$ to $t = n$);

(vii) the forecasts of the sea level are then obtained by summing the forecast sea level in first differences.

We also compute forecasts with the combinations: $n_{ed} = 60/n_{bin} = 60$, $n_{ed} = 60/n_{bin} = 180$, and $n_{ed} = 180/n_{bin} = 180$.

4.1.2 Vermeer and Rahmstorf (2009) procedure

The second competing method is the one used in Vermeer and Rahmstorf (2009). Their model is based on equation (16). The procedure is similar to the previous one, with the addition of an extra step, and it can be summarized as follows:

(i) the sea-level and temperature series, from time $t = 1$ up to $t = n^*$, are smoothed using singular spectrum analysis and an embedding dimension equal to $ed = 180$ months, corresponding to 15 years ($15 \times 12 = 180$), as used in the paper;

(ii) first differences of the smoothed sea-level series are then taken;

(iii) the smoothed series (temperature and first differences of the sea level) are then divided into 60 months bins, corresponding to 5 years ($5 \times 12 = 60$), as used in their paper, and in each bin the average is taken;

(iv) both time series of bin-averages are then detrended (by fitting a linear trend);

(v) the parameter v_2, in equation (16) (λ in the notation of their paper), is then selected as the value for which the correlation between the detrended bin-averages of the smoothed temperature and the detrended bin-averages of the first differences of the smoothed sea level, is maximized;

(vi) the bin-averages of the smoothed sea level in first differences are then regressed on the bin-averages of the smoothed temperature in levels, corrected for the rate of change of the temperature (that is the $v_2 \frac{dT(t)}{dt}$ factor in equation (16));

(vii) the estimated regression coefficients are then used to compute the values of the sea level in first differences from the out-of-sample (smoothed) temperatures, corrected for the $v_2 \frac{dT(t)}{dt}$ factor in equation (16), where the v_2 used is the one previously computed and the rate of change $\frac{dT(t)}{dt}$ is computed in the same way as before but from the out-of-sample (smoothed) temperatures (note that the information set used comprises the sea-level observations from time $t = 1$ to $t = n^*$ and observations of the temperature from $t = 1$ to $t = n$);

(viii) the forecasts of the sea level are then obtained by summing the forecast sea level in first differences.

We also compute forecasts with the combinations: $n_{ed} = 60/n_{bin} = 60$, $n_{ed} = 60/n_{bin} = 180$, and $n_{ed} = 180/n_{bin} = 180$.

4.1.3 Performance measure

As a measure of the relative forecasting power between the models, we take the ratios of the square roots of the mean squared forecast errors, from the different models. For model j we have:

$$R_f^j = \sqrt{\frac{1}{f} \sum_{h=1}^{f} \left(\hat{S}_{n^*+h}^j - S_{n^*+h}^r \right)}, \tag{35}$$

where $\hat{S}_{n^*+h}^j$ denotes the sea-level forecast from the j-th model and $S_{n^*+h}^r$ is the observed sea level[13]. We select different values of n^*. Note that in computing R_f^j we are giving equal weight to forecasts at different horizons. This strategy is motivated by the final goal of the model, that is to make long-term projections of the sea level. To compare the models, we take ratios between the R measures, equation (35), from the different forecasting models/methods.

[13]The superscript r stands for "reconstructed", as the observations are a reconstruction of the sea-level series, made from different measurements of the sea level.

4.2 Forecasting conditional on AR4-IPCC temperature scenarios

In this subsection we explain the method used to make long-term projections for the sea level, conditional on the IPCC temperature scenarios. First, note that the measurements of sea level and temperature go from January 1880 to December 2009 and correspond to monthly averages, whereas the IPCC temperature scenarios, ranging from 2010 to 2099, correspond to yearly values. In order to model the data and the scenarios in the same framework, we transform the yearly values in monthly ones. In particular, for each scenario we treat the temperature value corresponding to a specific year, as an observation for the month of July for that year, treating the values for the remaining months as missing values.

Denote with n^{tot} the sample size of the assembled dataset made up of the monthly observations of sea level and temperatures plus the IPCC temperature scenarios, in particular we have $n^{tot} = 1560 + 1080 = 2640$. To construct the sea-level forecasts, conditional on the temperature scenarios, we follow these steps:

(i) estimate the system parameters by maximum likelihood using observations of sea level and temperature from time $t = 1$ up to time $t = n$;

(ii) run the Kalman filter, using the estimated parameters, on the dataset composed of observations of the sea level and temperature from time $t = 1$ to $t = n$, and *one* temperature scenario from $t = n + 1$ to $t = n^{tot}$;

(iii) the forecasts of the sea level are then the smoothed values $\hat{S}_{n+h}$ with $h = 1, \ldots, n^{tot} - n$.

The procedure is repeated for each of the 75 temperature scenarios. In order to compute confidence intervals for the sea-level projections, we first use a bootstrap procedure to obtain an empirical distribution function (EDF) for the forecasts, conditioning on each scenario separately. We then aggregate these EDFs using the law of total probabilities, assigning equal probability to the different scenarios. Denoting with B_i the i-th IPCC temperature scenario, where $i = 1, \ldots, N$ ($N = 75$) and with h the forecast horizon, the unconditional empirical distribution function for the sea-level projections is

$$\begin{aligned} Pr\left(\hat{S}_{t+h} \leq s\right) &= \sum_{i=1}^{N} Pr\left(\hat{S}_{t+h} \leq s | B_i\right) Pr\left(B_i\right) \\ &= \frac{1}{N} \sum_{i=1}^{N} Pr\left(\hat{S}_{t+h} \leq s | B_i\right), \end{aligned} \tag{36}$$

where $Pr(\hat{S}_{t+h} \leq s|B_i)$ is the conditional distribution function of the sea-level forecast $\hat{S}_{t+h}$, given a temperature scenario B_i, and $Pr(B_i)$ is the probability of the i-th temperature scenario. The confidence intervals for the forecasts $\hat{S}_{t+h}$ are then obtained by taking the 1st and 99th percentiles of the cumulative distribution function $Pr(\hat{S}_{t+h} \leq s)$. The EDFs $Pr(\hat{S}_{t+h} \leq s|B_i)$ are obtained using a bootstrap procedure, and the probabilities $Pr(B_i)$ are set equal to $1/N$. We thus assume equal probabilities for the different temperature scenarios, in line with the literature.

The bootstrap procedure is detailed in Appendix B and it is a modification of the method proposed in Rodriguez and Ruiz (2009). In Rodriguez and Ruiz (2009), they consider a time invariant state-space system in which the system parameters do not vary in time. In the present paper, however, we assume a time-varying measurement noise variance for the sea level $\sigma_t^{2,S}$ (33), this introduces heteroskedasticity in the innovations.

5 Computational aspects

The parameters of the state-space system are estimated by maximum likelihood. The likelihood function is delivered by the Kalman filter. We employ the univariate Kalman filter derived in Koopman and Durbin (2000), as we assume a diagonal covariance matrix for the innovations in the measurement equation. The maximum of the likelihood function has no explicit form solution and numerical methods have to be employed. We make use of two algorithms:

- **CMA-ES**. Covariance Matrix Adaptation Evolution Strategy, see Hansen and Ostermeier (1996)[14]. This is a genetic algorithm that samples the parameter space according to a Gaussian search distribution, which changes according to where the best solutions are found in the parameter space;

- **BFGS**. Broyden-Fletcher-Goldfarb-Shanno, see for instance Press et al. (2002). This algorithm belongs to the class of quasi-Newton methods and requires the computation of the gradient of the function to be minimized.

The CMA-ES algorithm performs very well when no good initial values are available but it is slower to converge than the BFGS routine. The BFGS algorithm, on the other hand, requires good initial values but converges considerably faster than the CMA-ES algorithm (once good initial values have been obtained). Hence, we use the CMA-ES algorithm to find good initial values and then the BFGS one to perform the minimizations with the different sample sizes, needed in the forecasting exercise detailed in Section 4.

To gain speed we choose C++ as the programming language, using routines from the Numerical Recipes, Press et al. (2002). We compile and run the executables on a Linux 64-bit operating system using the GCC compiler [15]. The integrals appearing in equations (31) can be computed analytically with the aid, for instance, of MATLAB® symbolic toolbox. The generated code can then be directly converted into C++ code with the command `ccode`.

6 Results and discussion

6.1 Model comparison results

To compute the out-of-sample forecasts for model (34) we use the Kalman filter, treating the sea-level values as missing observations, for the time points at which we want to forecast it. In the tables 1-4 in Appendix D are reported the ratios (35) for different values

[14] See `https://www.lri.fr/~hansen/cmaesintro.html` for references and source codes. The authors provide C source code for the algorithm which can be easily converted into C++ code.

[15] See `http://gcc.gnu.org/onlinedocs/` for more information on the Gnu Compiler Collection, GCC.

of the estimation sample n^* and forecast sample f. We label the different forecasting models according to the following convention.

- **model 1**. State-space system (22) with linear trend (24), taking the filtered values as forecasts;
- **model 2**. State-space system (22) with linear trend (24), taking the smoothed values as forecasts;
- **model 3**. State-space system (22) with quadratic trend (25), taking the filtered values as forecasts;
- **model 4**. State-space system (22) with quadratic trend (25), taking the smoothed values as forecasts;
- **model 5**. Rahmstorf (2007b) procedure (see Section 4.1.1) with embedding dimension $n_{ed} = 60$ and number of bins $n_{bin} = 60$;
- **model 6**. Rahmstorf (2007b) procedure (see Section 4.1.1) with embedding dimension $n_{ed} = 60$ and number of bins $n_{bin} = 180$;
- **model 7**. Rahmstorf (2007b) procedure (see Section 4.1.1) with embedding dimension $n_{ed} = 180$ and number of bins $n_{bin} = 60$;
- **model 8**. Rahmstorf (2007b) procedure (see Section 4.1.1) with embedding dimension $n_{ed} = 180$ and number of bins $n_{bin} = 180$;
- **model 9**. Vermeer and Rahmstorf (2009) procedure (see Section 4.1.2) with embedding dimension $n_{ed} = 60$ and number of bins $n_{bin} = 60$;
- **model 10**. Vermeer and Rahmstorf (2009) procedure (see Section 4.1.2) with embedding dimension $n_{ed} = 60$ and number of bins $n_{bin} = 180$;
- **model 11**. Vermeer and Rahmstorf (2009) procedure (see Section 4.1.2) with embedding dimension $n_{ed} = 180$ and number of bins $n_{bin} = 60$;
- **model 12**. Vermeer and Rahmstorf (2009) procedure (see Section 4.1.2) with embedding dimension $n_{ed} = 180$ and number of bins $n_{bin} = 180$.

It can be seen from tables 1-4 that the state-space models 1-2 and 3-4 perform quite well compared to models 5-12. In particular, the quadratic trend component (in models 3-4) seems to help the forecasting performance of the state-space system. The difference between the filtered and smoothed forecasts is negligible. These results show that similar (or better) forecasts can be obtained using the state-space systems presented in Section 2.3, compared to the two benchmark procedures outlined in Section 4.

We also considered specifications without trend components, with stochastic trends, and/or with various sets of coefficients restricted to zero. All these alternative specifications were found to perform poorly compared to the ones presented in this paper, in terms of forecasting performance. In particular, setting the coefficient $a^{SS} = 0$ or adding stochastic components in the trend process, considerably worsened the forecast performance of the models.

6.2 Full sample estimation results

In this subsection we present the parameter estimates relative to models 1-2 and models 3-4. The estimation results are contained in tables 5-6 (for models 1-2) and in tables 7-9 (for models 3-4) and they are divided into estimates for the continuous-time and discrete-time specifications. The tables can be found in Appendix D. We estimate the parameters using the complete dataset of sea-level and temperature monthly observations, ranging from January 1880 to December 2009, for a sample size equal to 1560. We group the comments according to the different models (1-2 and 3-4):

- **models 1-2**. The estimated standard deviation of the temperature measurement error is $\sigma^T = 7.59[cK]$ $(0.0759[K])$, which is slightly lower than the average standard deviation of the sea-level measurement errors $\overline{\sigma^S} = 11.43[mm]$ $(0.01143[m])$. The average $\overline{\sigma^S}$ is computed from the sequence of volatilities $\{\sigma^S_\tau\}_{\tau=1:n}$, corresponding to the uncertainty estimates reported in Church and White (2011). The autoregressive coefficients $A^{*,SS} = 0.99$ and $A^{*,TT} = 0.92$ are both close to unity. The coefficient linking sea level to temperature is found to be quite small, $A^{*,ST} = 0.0054[mm/cK]$ $(0.00054[m/K])$, whereas the one linking temperature to the sea level $A^{*,TS} = 0.0489[cK/mm]$ $(0.489[K/m])$ is quite large.

- **models 3-4**. The estimated standard deviation of the temperature measurement error is $\sigma^T = 7.41[cK]$ $(0.0741[K])$. The autoregressive coefficients $A^{*,SS} = 0.97$ and $A^{*,TT} = 0.89$ are both close to unity. Interestingly, the coefficients linking sea level to temperature, and vice versa, are found to have a negative sign $A^{*,ST} = -0.0035[mm/cK]$ $(-0.00035[m/K])$, $A^{*,TS} = -0.0426[cK/mm]$ $(-0.426[K/m])$.

The parameter a^{ST}, if left unrestricted, is estimated to be either positive or negative (depending on the model and the estimation sample) and of the order of $10^{-2}[mm/cK]$ $(10^{-3}[m/K])$ for a one month time-step. The low value of this parameter may be caused by long response times of the sea level to the temperature and the fact that the time-step considered is quite small. Early studies indicate lags in the order of 20 years, between temperature and sea-level rise, Gornitz et al. (1982). One puzzling fact is the change in sign of a^{ST} and a^{TS} between models 1-2 and 3-4.

We found that when the parameter a^{SS} is left unconstrained, the coefficient linking sea level and temperature is estimated to be very low. This may suggest long response times of the sea level to the temperature changes, possible distortions in the sea level and temperature reconstructions, and/or a misspecification of the functional link between the two variables.

One interesting finding concerns the role of the sea-level measurement error variance $\sigma^{2,S}_\tau$ in the state-space system. Namely, this parameter regulates the smoothness of the filtered (and smoothed) sea-level series. Interestingly, if $\sigma^{2,S}_\tau = \sigma^{2,S}$ is left unrestricted and estimated together with the other parameters, the value obtained is very close to zero. This causes the filtered (and smoothed) sea-level series to essentially coincide with the observed ones. Intuitively, in this case the forecasts worsen.

6.3 Forecasting conditional on AR4-IPCC scenarios results

In this subsection we report the long-term sea-level projections, computed conditionally on the different temperature scenarios. See Section 4.2 for more details on the forecasting

procedure and Section 3 for a description of the temperature scenarios used. The scenarios are depicted in figure 1. We make sea-level rise projections using models 2 and 4, with respect to the (smoothed) sea-level value in 2009:

- **model 2**. The forecasts are quite sensitive to the temperature scenarios. Denote with $q_{0.01}$ and $q_{0.99}$ the 1st and 99th percentiles of the distribution of sea-level forecasts for the year 2099. If we condition on all of the 75 temperature scenarios, taken with equal probability, the sea-level forecasts range from $q_{0.01} = 0.0948[m]$ to $q_{0.99} = 0.3525[m]$ with a mean value of $0.2130[m]$, see figure 2. This range changes if different scenario groups are considered separately.

  (i) **A1b group**: forecasts range from $q_{0.01} = 0.1829[m]$ to $q_{0.99} = 0.3537[m]$ with a mean value of $0.2470[m]$;

  (ii) **A2 group**: forecasts range from $q_{0.01} = 0.2030[m]$ to $q_{0.99} = 0.3654[m]$ with a mean value of $0.2845[m]$;

  (iii) **B1 group**: forecasts range from $q_{0.01} = 0.1485[m]$ to $q_{0.99} = 0.2688[m]$ with a mean value of $0.1941[m]$;

  (iv) **commit group**: forecasts range from $q_{0.01} = 0.0868[m]$ to $q_{0.99} = 0.1489[m]$ with a mean value of $0.1174[m]$.

- **model 4**. The forecasts are not very sensitive to the temperature scenarios. In particular, the forecasts relative to 2099 for the sea level range between $q_{0.01} = 0.1999[m]$ and $q_{0.99} = 0.2817[m]$, with a mean value of $0.2410[m]$, conditioning on all temperature scenarios, taken with equal probability, see figure 3. This range does not change much if different groups are considered separately.

  (i) **A1b group**: forecasts range from $q_{0.01} = 0.1991[m]$ to $q_{0.99} = 0.2696[m]$ with a mean value of $0.2375[m]$;

  (ii) **A2 group**: from $q_{0.01} = 0.1886[m]$ to $q_{0.99} = 0.2704[m]$ with a mean value of $0.2341[m]$;

  (iii) **B1 group**: from $q_{0.01} = 0.2121[m]$ to $q_{0.99} = 0.2738[m]$ with a mean value of $0.2428[m]$;

  (iv) **commit group**: from $q_{0.01} = 0.2072[m]$ to $q_{0.99} = 0.2944[m]$ with a mean value of $0.2507[m]$.

The difference between the average, smoothed sea level in 1990 and the smoothed sea level in December 2009 is $0.0549[m]$. Consequently, to compute the sea-level changes with respect to the average 1990 level, $0.0549[m]$ has to be added to the previous values. We make this remark because in several papers the sea-level rise forecasts are reported with respect to the 1990 average, e.g. in Rahmstorf (2007b), Vermeer and Rahmstorf (2009), and Grinsted et al. (2010).

Figure 1: AR4-IPCC tempterature scenarios.

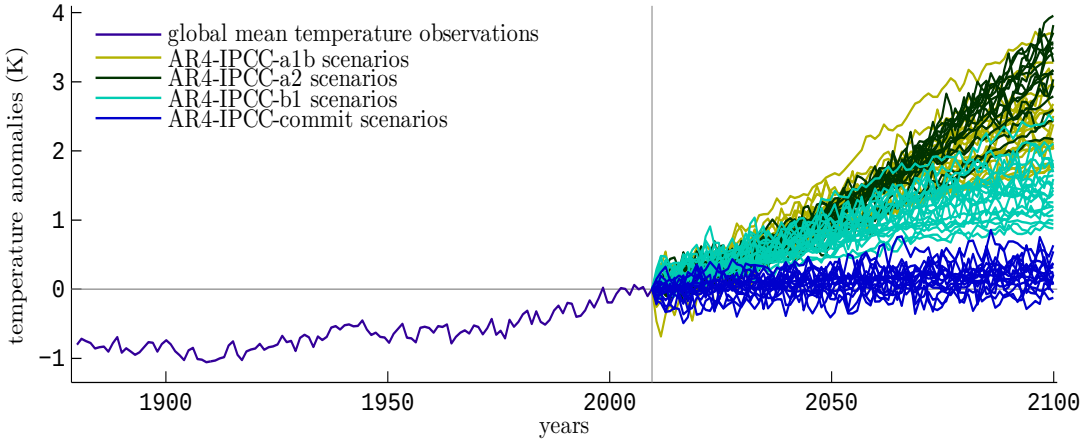

Temperature observations and AR4-IPCC-SRES tempterature scenarios. The temperature observations are yearly averages, ranging from January 1880 to December 2009. The AR4-IPCC-SRES scenarios correspond to yearly simulated values, ranging from January 2010 to December 2099.

Figure 2: Forecasts based on A1b-A2-B1-commit-IPCC scenarios and model 2.

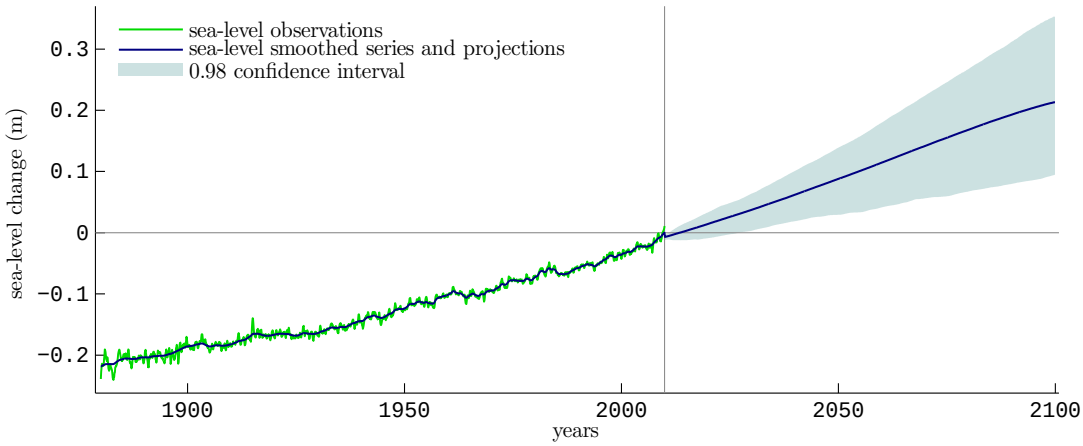

Forecasts based on IPCC-SRES (A1b, A2, B1, and commit groups) scenarios and model 2 (see Section 4.2). The observations and the projections are monthly values. The sea-level observations range from January 1880 to December 2009. The projections correspond to smoothed monthly values and range from January 2010 to December 2099. The base sea-level value is the smoothed sea level in December 2009. The confidence bands correspond to a 98% confidence interval (see Section 4.2).

Figure 3: Forecasts based on A1b-A2-B1-commit-IPCC scenarios and model 4.

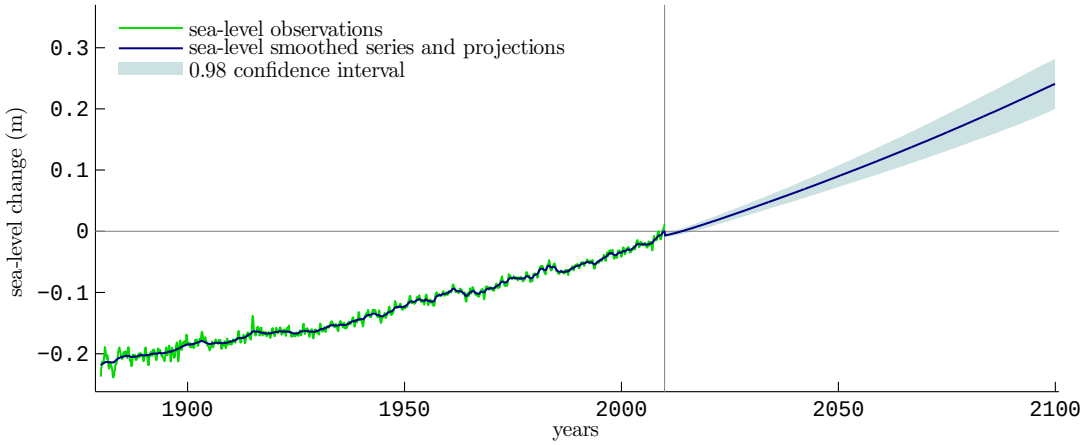

Forecasts based on IPCC-SRES (A1b, A2, B1, and commit groups) scenarios and model 4 (see Section 4.2). The observations and the projections are monthly values. The sea-level observations range from January 1880 to December 2009. The projections correspond to smoothed monthly values and range from January 2010 to December 2099. The base sea-level value is the smoothed sea-level in December 2009. The confidence bands correspond to a 98% confidence interval (see Section 4.2).

7 Conclusions

In this paper we proposed a statistical framework to model and forecast the global mean sea level, conditional on the global mean temperature. The specification is formulated as a continuous-time state-space system. The state vector is composed of the unobserved sea level and temperature processes, as well as trend components and, jointly, follow an Ornstein-Uhlenbeck process. This process can be exactly discretised. The measurement equation adds independent noise to the discretely sampled states. The resulting system is linear and Kalman filtering techniques apply. In particular, the Kalman filter is used to compute the likelihood function. Furthermore, we exploit the ability of the Kalman filter to deal with missing observations, to make projections for the sea level. The state-space specification also allows to model changes in the accuracy of the reconstructed sea-level series. Specifically, this is achieved by allowing the volatility parameter of the sea-level measurement error to be time-varying, and matching it to the sea-level uncertainty values reported in Church and White (2011). We find that this modelling scheme performs better, in forecasting, compared to one in which the volatility of the measurement error of the sea level is estimated together with the other parameters. If $\sigma_\tau^{2,S} = \sigma^{2,S}$ is left unrestricted and estimated together with the other parameters, the value obtained is very close to zero. This causes the filtered (and smoothed) sea-level series to essentially coincide with the observed one. In this case the predictive ability of the model deteriorates. The advantage of using the proposed state-space model is that there is no difference between the system dynamics assumed for the variables of interest and the statistical model estimated using real data.

The choice of the models was made according to their forecasting performance, relative to selected benchmarks, namely the Rahmstorf (2007b) and Vermeer and Rahmstorf (2009) methods. This model selection criterion was chosen because of the final objective

of semi-empirical models, that is making long-term projections for the sea level.

We find that the magnitude of the parameter $A^{*,ST}$, linking the sea level to the temperature, is estimated to be of the order of $10^{-2}[mm/cK]$ ($10^{-3}[m/K]$). Note that $A^{*,ST}$ relates the value of the unobserved temperature process at time τ to the value of the sea level at time $\tau+1$, where the time step corresponds to one month. The low value of $A^{*,ST}$ may be caused by long response times of the sea level to the temperature and the fact that the time step is quite short. Early studies indicate lags of the order of 20 years (240 months), between temperature and sea-level rise, see for instance Gornitz et al. (1982).

When the parameter a^{SS} is left unconstrained, the coefficient linking sea level and temperature is estimated to be very low. However, if the parameter a^{SS} is restricted to be zero, the forecast performance of the model deteriorates considerably. One puzzling fact is the change in sign of $A^{*,ST}$ and $A^{*,TS}$, between the linear and quadratic trend specifications. In particular, both parameters are positive in the linear trend specification and negative in the quadratic trend one. This finding is quite surprising, considering that the quadratic trend model seems to forecast better than the linear one. Concerning the model comparison exercise, the state-space specifications behave well compared to the Rahmstorf (2007b) and Vermeer and Rahmstorf (2009) methods. The choice of the trend component influences somewhat the forecasting performance of the model.

We make projections for the sea level from 2010 up to 2099. Under the linear trend specification the forecasts are quite sensitive to the temperature scenarios, whereas under the quadratic one the projections are quite similar across scenarios. Denote with $q_{0.01}$ and $q_{0.99}$ the 1st and 99th percentiles, respectively, of the distribution of sea-level rise forecasts for the year 2099 with respect to the (smoothed) sea-level value in 2009. Conditionally on all the 75 temperature scenarios, the sea-level rise forecasts range from $q_{0.01} = 0.0948[m]$ to $q_{0.99} = 0.3525[m]$, with a mean value of $0.2130[m]$ under the linear trend specification, and from $q_{0.01} = 0.1999[m]$ to $q_{0.99} = 0.2817[m]$, with a mean value of $0.2410[m]$, under the quadratic trend model. With respect to the mean, smoothed 1990 sea-level value, the above results translate into sea-level rise forecasts ranging from $q_{0.01} = 0.1497[m]$ to $q_{0.99} = 0.4074[m]$, with a mean value of $0.2679[m]$ under the linear trend specification, and from $q_{0.01} = 0.2548[m]$ to $q_{0.99} = 0.3366[m]$, with a mean value of $0.2959[m]$, under the quadratic trend model.

The projections obtained with the models proposed in this study are lower than the ones obtained in Rahmstorf (2007b), Vermeer and Rahmstorf (2009), and Grinsted et al. (2010). In particular, their projections for the year 2100, with respect to the mean sea level in 1990, range from $0.5[m]$ to $1.38[m]$ for Rahmstorf (2007b), from $0.72[m]$ to $1.81[m]$ for Vermeer and Rahmstorf (2009), and from $1.30[m]$ to $1.80[m]$ (or between $0.95[m]$ to $1.48[m]$, depending on the temperature reconstruction) for Grinsted et al. (2010). Note, however, that in these three papers the interpretation of the range spanned by the forecasts is different from ours. Most likely, we obtain lower estimates for the sea level because of the coefficient relating temperature to sea-level $A^{*,ST}$, which in the state-space specifications is estimated to be quite small. This implies longer estimated response times of the sea level to changes in the temperature, with respect to the aforementioned studies.

Possible continuations of this work could be represented by considering alternative continuous-time stochastic processes to model sea level and temperature, for instance geometric Brownian motions or more general Itô processes. Another important aspect in this analysis was the specification of the trend components, which played a key role in

the forecasting of the sea level. It would be interesting to study alternative specifications for the trend components and their relation to different climate forcings, such as human induced changes in greenhouse gases and aerosols concentrations.

References

Anthoff, D., R. J. Nicholls, and R. S. Tol (2010). The economic impact of substantial sea-level rise. *Mitigation and Adaptation Strategies for Global Change 15*(4), 321–335.

Anthoff, D., R. J. Nicholls, R. S. Tol, and A. T. Vafeidis (2006). Global and regional exposure to large rises in sea-level: a sensitivity analysis. *Tyndall centre for climate change research-Working Paper 96*.

Arnell, N., E. L. Tompkins, N. Adger, and K. Delaney (2005). Vulnerability to abrupt climate change in europe.

Bergstrom, A. R. (1997). Gaussian estimation of mixed-order continuous-time dynamic models with unobservable stochastic trends from mixed stock and flow data. *Econometric Theory 13*(04), 467–505.

Brockwell, P. J. and R. A. Davis (2009). *Time series: theory and methods*. Springer.

Budyko, M. I. (1968). On the origin of glacial epochs. *Meteorol. Gidrol 2*, 3–8.

Budyko, M. I. (1969). The effect of solar radiation variations on the climate of the earth. *Tellus 21*(5), 611–619.

Budyko, M. I. (1972). The future climate. *Eos, Transactions American Geophysical Union 53*(10), 868–874.

Cane, M. A., A. Kaplan, R. N. Miller, B. Tang, E. C. Hackert, and A. J. Busalacchi (1996). Mapping tropical pacific sea level: Data assimilation via a reduced state space kalman filter. *Journal of Geophysical Research: Oceans (1978–2012) 101*(C10), 22599–22617.

Carter, T. (2007). General guidelines on the use of scenario data for climate impact and adaptation assessment. Technical report, Task Group on Data and Scenario Support for Impact and Climate Assessment (TGICA), Intergovernmental Panel on Climate Change.

Cazenave, A. and R. S. Nerem (2004). Present-day sea level change: Observations and causes. *Reviews of Geophysics 42*(3).

Chan, N. H., J. B. Kadane, R. N. Miller, and W. Palma (1996). Estimation of tropical sea level anomaly by an improved kalman filter. *Journal of physical oceanography 26*(7), 1286–1303.

Church, J. A. and N. J. White (2006). A 20th century acceleration in global sea-level rise. *Geophysical research letters 33*(1).

Church, J. A. and N. J. White (2011). Sea-level rise from the late 19th to the early 21st century. *Surveys in Geophysics 32*(4-5), 585–602.

Durbin, J. and S. J. Koopman (2012). *Time series analysis by state space methods*. Oxford University Press.

Fraedrich, K. (1978). Structural and stochastic analysis of a zero-dimensional climate system. *Quarterly Journal of the Royal Meteorological Society 104*(440), 461–474.

Gornitz, V., S. Lebedeff, and J. Hansen (1982). Global sea level trend in the past century. *Science 215*(4540), 1611–1614.

Grinsted, A., J. C. Moore, and S. Jevrejeva (2010). Reconstructing sea level from paleo and projected temperatures 200 to 2100 ad. *Climate Dynamics 34*(4), 461–472.

Hansen, J., R. Ruedy, M. Sato, M. Imhoff, W. Lawrence, D. Easterling, T. Peterson, and T. Karl (2001). A closer look at united states and global surface temperature change. *Journal of Geophysical Research: Atmospheres (1984–2012) 106*(D20), 23947–23963.

Hansen, J., R. Ruedy, M. Sato, and K. Lo (2010). Global surface temperature change. *Reviews of Geophysics 48*(4).

Hansen, N. and A. Ostermeier (1996). Adapting arbitrary normal mutation distributions in evolution strategies: The covariance matrix adaptation. In *Evolutionary Computation, 1996., Proceedings of IEEE International Conference on*, pp. 312–317. IEEE.

Harvey, A. and J. H. Stock (1993). Estimation, smoothing, interpolation, and distribution for structural time-series models in continuous time. *Models, Methods and Applications of Econometrics*, 55–70.

Hasselmann, K. (1976). Stochastic climate models part i. theory. *Tellus 28*(6), 473–485.

Hay, C. C., E. Morrow, R. E. Kopp, and J. X. Mitrovica (2013). Estimating the sources of global sea level rise with data assimilation techniques. *Proceedings of the National Academy of Sciences 110*(Supplement 1), 3692–3699.

Holgate, S., S. Jevrejeva, P. Woodworth, and S. Brewer (2007). Comment on "a semi-empirical approach to projecting future sea-level rise". *Science 317*(5846), 1866–1866.

Imkeller, P. (2001). Energy balance modelsviewed from stochastic dynamics. In *Stochastic climate models*, pp. 213–240. Springer.

Jevrejeva, S., A. Grinsted, and J. Moore (2009). Anthropogenic forcing dominates sea level rise since 1850. *Geophysical Research Letters 36*(20).

Jevrejeva, S., J. Moore, and A. Grinsted (2010). How will sea level respond to changes in natural and anthropogenic forcings by 2100? *Geophysical research letters 37*(7).

Jevrejeva, S., J. C. Moore, and A. Grinsted (2012a). Potential for bias in 21st century semiempirical sea level projections. *Journal of Geophysical Research: Atmospheres (1984–2012) 117*(D20).

Jevrejeva, S., J. C. Moore, and A. Grinsted (2012b). Sea level projections to ad2500 with a new generation of climate change scenarios. *Global and Planetary Change 80*, 14–20.

Kemp, A. C., B. P. Horton, J. P. Donnelly, M. E. Mann, M. Vermeer, and S. Rahmstorf (2011). Climate related sea-level variations over the past two millennia. *Proceedings of the National Academy of Sciences*.

Koopman, S. J. and J. Durbin (2000). Fast filtering and smoothing for multivariate state space models. *Journal of Time Series Analysis 21*(3), 281–296.

Liu, R. Y. et al. (1988). Bootstrap procedures under some non-iid models. *The Annals of Statistics 16*(4), 1696–1708.

Mammen, E. (1993). Bootstrap and wild bootstrap for high dimensional linear models. *The Annals of Statistics*, 255–285.

Meehl, G. A., C. Covey, K. E. Taylor, T. Delworth, R. J. Stouffer, M. Latif, B. McAvaney, and J. F. Mitchell (2007). The wcrp cmip3 multimodel dataset: A new era in climate change research. *Bulletin of the American Meteorological Society 88*(9), 1383–1394.

Meehl, G. A., T. F. Stocker, W. D. Collins, P. Friedlingstein, A. T. Gaye, J. M. Gregory, A. Kitoh, R. Knutti, J. M. Murphy, A. Noda, et al. (2007). Global climate projections. *Climate change 283*.

Miller, R. N. and M. A. Cane (1989). A kalman filter analysis of sea level height in the tropical pacific.

Moore, J. C., A. Grinsted, T. Zwinger, and S. Jevrejeva (2013). Semiempirical and process-based global sea level projections. *Reviews of Geophysics 51*(3), 484–522.

Munk, W. (2002). Twentieth century sea level: An enigma. *Proceedings of the national academy of sciences 99*(10), 6550–6555.

Nicolis, C. (1982). Stochastic aspects of climatic transitionsresponse to a periodic forcing. *Tellus 34*(1), 1–9.

North, G. R., R. F. Cahalan, and J. A. Coakley (1981). Energy balance climate models. *Reviews of Geophysics 19*(1), 91–121.

Pardaens, A., J. Lowe, S. Brown, R. Nicholls, and D. De Gusmão (2011). Sea-level rise and impacts projections under a future scenario with large greenhouse gas emission reductions. *Geophysical Research Letters 38*(12).

Press, W. H., S. A. Teukolsky, W. T. Vetterling, and B. P. Flannery (2002). *Numerical Recipes in C++* (Second ed.). Cambridge University Press, Cambridge.

Pretis, F. (2015). Econometric methods to model non-stationary climate systems: the equivalence of two-component energy balance models and cointegrated VARs. Technical report, Institute for new economic thinking, Oxfor Martin School, University of Oxford.

Rahmstorf, S. (2007a). Response to comments on "a semi-empirical approach to projecting future sea-level rise". *Science 317*(5846), 1866d–1866d.

Rahmstorf, S. (2007b). A semi-empirical approach to projecting future sea-level rise. *Science 315*(5810), 368–370.

Rodriguez, A. and E. Ruiz (2009). Bootstrap prediction intervals in state–space models. *Journal of time series analysis 30*(2), 167–178.

Sellers, W. D. (1969). A global climatic model based on the energy balance of the earth-atmosphere system. *Journal of Applied Meteorology 8*(3), 392–400.

Solomon, S., G.-K. Plattner, R. Knutti, and P. Friedlingstein (2009). Irreversible climate change due to carbon dioxide emissions. *Proceedings of the national academy of sciences 106*(6), 1704–1709.

Sugiyama, M., R. J. Nicholls, and A. Vafeidis (2008). Estimating the economic cost of sea-level rise. Technical report, MIT Joint Program on the Science and Policy of Global Change.

Vermeer, M. and S. Rahmstorf (2009). Global sea level linked to global temperature. *Proceedings of the National Academy of Sciences 106*(51), 21527–21532.

Wu, C.-F. J. (1986). Jackknife, bootstrap and other resampling methods in regression analysis. *the Annals of Statistics*, 1261–1295.

Appendices

A Details of univariate Kalman filter

In this section we give details on the Kalman filter and its univariate version. The univariate Kalman filter was used for the computation of the likelihood function and for the bootstrap procedure, needed to compute prediction intervals for the sea-level projections, see Section 6.3. This subsection draws heavily on Durbin and Koopman (2012).

Consider the following state-space system

$$\begin{aligned} \boldsymbol{y}_t &= \mathbf{Z}\boldsymbol{\alpha}_t + \boldsymbol{\epsilon}_t, \\ \boldsymbol{\alpha}_{t+1} &= \mathbf{c} + \mathbf{T}\boldsymbol{\alpha}_t + \boldsymbol{\eta}_t, \end{aligned} \tag{37}$$

where $\boldsymbol{\epsilon}_t \sim N(\mathbf{0}, \mathbf{H}_t)$ takes values in $\mathbb{R}^p$, with $\mathbf{H}_t$ a covariance matrix, $\boldsymbol{\eta}_t \sim N(\mathbf{0}, \mathbf{Q})$ takes values in $\mathbb{R}^k$, with $\mathbf{Q}$ a covariance matrix, $\mathbf{y}_t \in \mathbb{R}^p$, $\boldsymbol{\alpha}_t \in \mathbb{R}^k$, and $\mathbf{Z}$, $\mathbf{T}$, and $\mathbf{c}$ are parameter matrices and vectors of appropriate dimensions. Notice that the state-space system (34) is of the same type as system (37). The standard Kalman filter recursions for system (37) are

$$\begin{aligned} \mathbf{v}_t &= \mathbf{y}_t - \mathbf{Z}\mathbf{a}_t, \\ \mathbf{F}_t &= \mathbf{Z}\mathbf{P}_t\mathbf{Z}' + \mathbf{H}_t, \\ \tilde{\mathbf{K}}_t &= \mathbf{P}_t\mathbf{Z}', \end{aligned} \tag{38}$$

$$\begin{aligned} \mathbf{a}_{t|t} &= \mathbf{a}_t + \tilde{\mathbf{K}}_t\mathbf{F}_t^{-1}\mathbf{v}_t, & \mathbf{P}_{t|t} &= \mathbf{P}_t - \tilde{\mathbf{K}}_t\mathbf{F}_t^{-1}\tilde{\mathbf{K}}_t', \\ \mathbf{a}_{t+1} &= \mathbf{T}_t\mathbf{a}_{t|t} + \mathbf{c}, & \mathbf{P}_{t+1} &= \mathbf{T}\mathbf{P}_{t|t}\mathbf{T}' + \mathbf{Q}, \end{aligned} \tag{39}$$

for $t = 1, \ldots, n$, where $\mathbf{P}_t = E\left[[\boldsymbol{\alpha}_t - \mathbf{a}_t][\boldsymbol{\alpha}_t - \mathbf{a}_t]'\right]$, $\mathbf{P}_{t|t} = E\left[[\boldsymbol{\alpha}_t - \mathbf{a}_{t|t}][\boldsymbol{\alpha}_t - \mathbf{a}_{t|t}]'\right]$, and $\mathbf{a}_t = E[\boldsymbol{\alpha}|\mathbf{y}_0, \ldots, \mathbf{y}_{t-1}]$ and $\mathbf{a}_{t|t} = E[\boldsymbol{\alpha}|\mathbf{y}_0, \ldots, \mathbf{y}_t]$ are the one-step-ahead prediction and the filtered states, respectively. Koopman and Durbin (2000) derived a univariate version of this algorithm in the case of diagonal variance-covariance matrices $\mathbf{H}_t$. In this case the system (37) can be represented as

$$\begin{aligned} y_{t,i} &= \mathbf{z}_i\boldsymbol{\alpha}_{t,i} + \epsilon_{t,i}, & t &= 1, \ldots, n \quad i = 1, \ldots, p, \\ \boldsymbol{\alpha}_{t,i+1} &= \boldsymbol{\alpha}_{t,i}, & t &= 1, \ldots, n \quad i = 1, \ldots, p-1, \\ \boldsymbol{\alpha}_{t,i+1} &= \mathbf{c} + \mathbf{T}\boldsymbol{\alpha}_{t,i} + \boldsymbol{\eta}_t, & t &= 1, \ldots, n \quad i = p. \end{aligned} \tag{40}$$

Where $\mathbf{z}_i$ is the $i-th$ row of matrix $\mathbf{Z}$, $y_{t,i}$ and $\epsilon_{t,i} \sim N(0, \sigma^2_{t,i})$ are the $i-th$ components of $\mathbf{y}_t$ and $\boldsymbol{\epsilon}_t$, respectively. The Kalman filter recursions for specification (40) can be written as

$$v_{t,i} = y_{t,i} - \mathbf{z}_i\mathbf{a}_{t,i}, \tag{41}$$

$$F_{t,i} = \mathbf{z}_i\mathbf{P}_{t,i}\mathbf{z}_i' + \sigma^2_{t,i}, \tag{42}$$

$$\tilde{\mathbf{k}}_{t,i} = \mathbf{P}_{t,i}\mathbf{z}_i', \tag{43}$$

$$\left.\begin{aligned} \mathbf{a}_{t,i+1} &= \mathbf{a}_{t,i} + \tilde{\mathbf{k}}_{t,i}F_{t,i}^{-1}v_{t,i} \\ \mathbf{P}_{t,i+1} &= \mathbf{P}_{t,i} - \tilde{\mathbf{k}}_{t,i}F_{t,i}^{-1}\tilde{\mathbf{k}}_{t,i}' \end{aligned}\right\} \quad \text{for } i = 1, \ldots, p-1 \;\; t = 1, \ldots, n, \tag{44}$$

$$\left.\begin{aligned} \mathbf{a}_{t+1,1} &= \mathbf{T}(\mathbf{a}_{t,i} + \tilde{\mathbf{k}}_{t,i}F_{t,i}^{-1}v_{t,i}) + \mathbf{c} \\ \mathbf{P}_{t+1,1} &= \mathbf{T}(\mathbf{P}_{t,i} - \tilde{\mathbf{k}}_{t,i}F_{t,i}^{-1}\tilde{\mathbf{k}}_{t,i}')\mathbf{T}' + \mathbf{Q} \end{aligned}\right\} \quad \text{for } i = p \quad t = 1, \ldots, n. \tag{45}$$

Notice that $F_{t,i}$ is a scalar. As a consequence the univariate recursions do not require the inversion of $p \times p$ matrices, as in the standard Kalman filter recursions (38)-(39) and can lead to computational savings.

The state-space system (40) has two types of disturbances, namely $\epsilon_{t,i}$, and $\boldsymbol{\eta}_t$. The so called "innovation form" has a unique source of disturbance, that is $v_{t,i}$. The innovation form is made up of the following equations:

$$\begin{aligned}
y_{t,i} &= \mathbf{z}_i \mathbf{a}_{t,i} + v_{t,i}, \\
\mathbf{k}_{t,i} &= \mathbf{P}_{t,i} \mathbf{z}_i', \\
\mathbf{a}_{t,i+1} &= \mathbf{a}_{t,i} + \mathbf{k}_{t,i} F_{t,i}^{-1} v_{t,i}, \qquad \text{for } i = 1, 2, \ldots, p-1 \quad t = 1, 2, \ldots, n, \\
\mathbf{a}_{t+1,1} &= \mathbf{T} \left(\mathbf{a}_{t,i} + \mathbf{k}_{t,i} F_{t,i}^{-1} v_{t,i} \right) + \mathbf{c}, \qquad \text{for } i = p \quad t = 1, 2, \ldots, n.
\end{aligned} \tag{46}$$

The innovation form (46) of the state-space system (40) constitutes the basis for the bootstrap procedure outlined in the following subsection.

B Bootstrap procedure

In this section we outline the bootstrap procedure used to compute the prediction intervals for the sea-level projections, conditional on the IPCC scenarios, as described in Section 6.3. We detail the algorithm with respect to the state-space system (37) and the Kalman filter recursions (41)-(45). The algorithm is a modification of the one proposed in Rodriguez and Ruiz (2009) that allows for time-varying measurement error variances. Denote with $\boldsymbol{\theta}$ the vector containing the parameters of the state-space system (37). The algorithm we propose is made up of the following steps:

1. estimate the parameters of model (30) by maximum likelihood and obtain $\hat{\boldsymbol{\theta}}$ and the sequence of innovations $\{v_{t,i}\}_{t=1,\dots,n}^{i=1,\dots,p}$;

2. compute the centred innovations $\{v_{t,i}^c\}_{t=1,\dots,n}^{i=1,\dots,p}$, obtained as $v_{t,i}^c = v_{t,i} - \bar{v}_{n,i}$, with $\bar{v}_{n,i} = (1/n)\sum_{t=1}^{n} v_{t,i}$;

3. obtain the standardized innovations $\{v_{t,i}^s\}_{t=1,\dots,n}^{i=1,\dots,p}$, computed as $v_{t,i}^s = \frac{v_{t,i}^c}{\sqrt{F_{t,i}}}$;

4. obtain a sequence of bootstrap standardized innovations $\{v_{t,i}^*\}_{t=1,\dots,n}^{i=1,\dots,p}$ via random draws with replacement from the randomly scaled standardized innovations $\{v_{t,i}^s \cdot \epsilon_{t,i}\}_{t=1,\dots,n}^{i=1,\dots,p}$, where $\epsilon_{t,i} \sim N(0,1)$;

5. compute a bootstrap replicate of the observations $\{y_{t,i}^*\}_{t=1,\dots,n}^{i=1,\dots,p}$ by means of the innovation form (46) using $\{v_{t,i}^*\}_{t=1,\dots,n}^{i=1,\dots,p}$ and the estimated parameters $\hat{\boldsymbol{\theta}}$;

6. estimate the corresponding bootstrap parameters $\hat{\boldsymbol{\theta}}^*$ from the bootstrap replicates;

7. run the Kalman filter with $\hat{\boldsymbol{\theta}}^*$ using the original observations and one temperature scenario as described in Section 4.2.

Steps 1-7 are repeated $N = 500$ for each temperature scenario. As made clear in step 4 we make use of a wild bootstrap procedure as opposed to the simple re-sampling method used in Rodriguez and Ruiz (2009). The wild bootstrap was originally proposed by Wu (1986) and it is well known in the literature to perform better than a simple resampling scheme in the presence of heteroskedasticity, see for instance Liu et al. (1988) and Mammen (1993). In this paper the heteroskedasticity comes from the time varying matrix $\mathbf{H}_t$. Note that the variance of the innovations $v_{t,i}$ is given by $F_{t,i} = \mathbf{z}_i \mathbf{P}_{t,i} \mathbf{z}_i' + \sigma_{t,i}^2$ where $\sigma_{t,i}^2$ is time-varying. In the notation of equation (33), it's the parameter $\sigma_t^{2,S}$ that causes the innovations $v_{t,i}$, in equation (41), to be heteroskedastic.

C State-space system and dimensional analysis

In this section we rewrite the state-space system (22) with linear trend (24), making clear the fundamental dimensions and the units of measurement of the quantities involved. We make use of SI units apart from the time dimension, for which we use months (or years). The time series of the sea level is in millimetres $[mm]$ and the temperature one is in centikelvin $[cK]$.

C.1 Continuous-time state equation

The continuous-time process driving the state equation has the following dimensions:

$$
\begin{aligned}
d\begin{bmatrix} {}^{[mm]}S(t) \\ {}^{[cK]}T(t) \\ {}^{[mm]}\mu^S(t) \\ {}^{[cK]}\mu^T(t) \end{bmatrix} &= \begin{bmatrix} 0 \\ 0 \\ [\frac{mm}{month}] \\ \lambda^S \\ [\frac{mm}{month}] \\ \lambda^T \end{bmatrix} {}^{[month]}dt \\
&+ \begin{bmatrix} [\frac{1}{month}] & [\frac{mm}{cK\cdot month}] & [\frac{1}{month}] & \\ a^{SS} & a^{ST} & \kappa^S & 0 \\ [\frac{cK}{mm\cdot month}] & [\frac{1}{month}] & & [\frac{1}{month}] \\ a^{TS} & a^{TT} & 0 & \kappa^T \\ 0 & 0 & 0 & 0 \\ 0 & 0 & 0 & 0 \end{bmatrix} \begin{bmatrix} {}^{[mm]}S(t) \\ {}^{[cK]}T(t) \\ {}^{[mm]}\mu^S(t) \\ {}^{[cK]}\mu^T(t) \end{bmatrix} {}^{[month]}dt \\
&+ \begin{bmatrix} 1 & 0 \\ 0 & 1 \\ 0 & 0 \\ 0 & 0 \end{bmatrix} \begin{bmatrix} {}^{[mm]}d\eta^S(t) \\ {}^{[cK]}d\eta^T(t) \end{bmatrix},
\end{aligned} \tag{47}
$$

denoting with $d\boldsymbol{\eta}(t) = [d\eta^S(t) : d\eta^T(t)]$, we have $E[d\boldsymbol{\eta}(t)d\boldsymbol{\eta}(t)'] = \boldsymbol{\Sigma}dt$, with $\boldsymbol{\Sigma}$ a symmetric positive semidefinite matrix. To understand the units of measurement of the components of $\boldsymbol{\Sigma}$ we can reason in the following way: first, write $E[d\boldsymbol{\eta}(t)d\boldsymbol{\eta}(t)'] = E[\sqrt{\boldsymbol{\Sigma}}d\mathbf{W}(t)d\mathbf{W}(t)'\sqrt{\boldsymbol{\Sigma}}']$ where $\sqrt{\boldsymbol{\Sigma}}$ represents a square root of the matrix $\boldsymbol{\Sigma}$ and $d\mathbf{W}(t) = [dW^S(t) : dW^T(t)]'$ is a two-dimensional Brownian motion such that

$$
E[d\mathbf{W}(t)d\mathbf{W}(t)'] = \begin{bmatrix} 1 & \rho \\ \rho & 1 \end{bmatrix} dt, \tag{48}
$$

where $|\rho| < 1$; second, denote

$$
\sqrt{\boldsymbol{\Sigma}} = \begin{bmatrix} \omega^{SS} & \omega^{ST} \\ \omega^{TS} & \omega^{TT} \end{bmatrix}, \tag{49}
$$

we can write

$$
\sqrt{\boldsymbol{\Sigma}}d\mathbf{W}(t) = \begin{bmatrix} \omega^{SS}dW^S(t) + \omega^{ST}dW^T(t) \\ \omega^{TS}dW^S(t) + \omega^{TT}dW^T(t) \end{bmatrix}, \tag{50}
$$

and

$$E\left[\sqrt{\boldsymbol{\Sigma}}d\mathbf{W}(t)d\mathbf{W}(t)'\sqrt{\boldsymbol{\Sigma}}'\right] = \begin{bmatrix}\Sigma^{SS} & \Sigma^{ST}\\ \Sigma^{TS} & \Sigma^{TT}\end{bmatrix}dt, \tag{51}$$

where

$$\begin{aligned}\Sigma^{SS}dt &= E\left[(\omega^{SS}dW^S)^2+(\omega^{ST}dW^T)^2+2\omega^{SS}\omega^{ST}dW^SdW^T\right]\\ &= (\omega^{SS})^2dt+(\omega^{ST})^2dt+2\omega^{SS}\omega^{ST}\rho dt\\ &= \left[(\omega^{SS})^2+(\omega^{ST})^2+2\omega^{SS}\omega^{ST}\rho\right]dt,\end{aligned} \tag{52}$$

and

$$\begin{aligned}\Sigma^{ST}dt &= E\left[\omega^{SS}\omega^{TS}(dW^S(t))^2+\omega^{ST}\omega^{TS}dW^S(t)dW^T(t)\right]\\ &+ E\left[\omega^{SS}\omega^{TT}dW^S(t)dW^T(t)+\omega^{ST}\omega^{TT}dW^T(t)dW^T(t)\right]\\ &= \omega^{SS}\omega^{TS}dt+\omega^{ST}\omega^{TS}\rho dt\\ &+ \omega^{SS}\omega^{TT}\rho dt+\omega^{ST}\omega^{TT}dt\\ &= \left[\omega^{SS}\omega^{TS}+\omega^{ST}\omega^{TS}\rho+\omega^{SS}\omega^{TT}\rho+\omega^{ST}\omega^{TT}\right]dt,\end{aligned} \tag{53}$$

from equation (52) we can deduce that ω^{SS} and ω^{ST} have units of measurement corresponding to $[mm/\sqrt{month}]$; to see this set $\omega^{ST}=0$ in equation 52, we have then $\Sigma^{SS}dt=(\omega^{SS})^2dt$ which has units of measurement of $[mm^2]$, as it is the expectation of the square of a quantity with units $[mm]$, this implies that $(\omega^{SS})^2$ and Σ^{SS} have units of $[mm^2/month]$, as time is measured in months $[month]$; from equation (52) it is also clear that ω^{ST} has the same units as ω^{SS}. Using the same line of reasoning we deduce that $(\omega^{TT})^2$, $(\omega^{TS})^2$, and Σ^{TT} have units of $[cK^2/month]$. Having recovered the units of measurement of ω^{SS}, ω^{ST}, ω^{TS}, and ω^{TT} we can deduce from equation (53) that the units of measurement of Σ^{ST} and Σ^{TS} are $[(mm\cdot cK)/month]$. In summary we obtain:

$$\boldsymbol{\Sigma} = \begin{bmatrix}\left[\frac{mm^2}{month}\right] & \left[\frac{mm\cdot cK}{month}\right]\\ \Sigma^{SS} & \Sigma^{ST}\\ \left[\frac{cK\cdot mm}{month}\right] & \left[\frac{cK^2}{month}\right]\\ \Sigma^{TS} & \Sigma^{TT}\end{bmatrix}. \tag{54}$$

C.2 Discrete-time state vector and measurement equation

The discretized state vector has the following dimensions:

$$\begin{bmatrix}[mm]\\ S_{\tau+1}\\ [cK]\\ T_{\tau+1}\\ [mm]\\ \mu^S_{\tau+1}\\ [cK]\\ \mu^T_{\tau+1}\end{bmatrix} = \begin{bmatrix}[mm]\\ c^{*,S}\\ [cK]\\ c^{*,T}\\ [mm]\\ c^{*,\mu^S}\\ [cK]\\ c^{*,\mu^T}\end{bmatrix} + \begin{bmatrix} & \left[\frac{mm}{cK}\right] & & \left[\frac{mm}{cK}\right]\\ A^{*,SS} & A^{*,ST} & A^{*,S\mu^S} & A^{*,S\mu^T}\\ \left[\frac{cK}{mm}\right] & & \left[\frac{cK}{mm}\right] & \\ A^{*,TS} & A^{*,TT} & A^{*,T\mu^S} & A^{*,T\mu^T}\\ 0 & 0 & 1 & 0\\ 0 & 0 & 0 & 1\end{bmatrix}\begin{bmatrix}[mm]\\ S_\tau\\ [cK]\\ T_\tau\\ [mm]\\ \mu^S_\tau\\ [cK]\\ \mu^T_\tau\end{bmatrix}$$
$$+ \begin{bmatrix}[mm]\\ \xi^S_\tau\\ [cK]\\ \xi^T_\tau\\ 0\\ 0\end{bmatrix}, \tag{55}$$

denoting $\bar{\boldsymbol{\xi}}_\tau = [\xi_\tau^S : \xi_\tau^T]'$, we have

$$E\left[\bar{\boldsymbol{\xi}}_\tau \bar{\boldsymbol{\xi}}_\tau'\right] = \begin{bmatrix} \underset{\sum^{*,SS}}{\left[mm^2\right]} & \underset{\sum^{*,ST}}{[mm \cdot cK]} \\ \underset{\sum^{*,TS}}{[cK \cdot mm]} & \underset{\sum^{*,TT}}{\left[cK^2\right]} \end{bmatrix}, \tag{56}$$

where the units of measurement were obtained by following the same logic as in the previous section.

Finally, the measurement equation has the following dimensions:

$$\begin{bmatrix} [mm] \\ S_\tau^r \\ [cK] \\ T_\tau^r \end{bmatrix} = \begin{bmatrix} 1 & 0 & 0 & 0 \\ 0 & 1 & 0 & 0 \end{bmatrix} \begin{bmatrix} [mm] \\ S_\tau \\ [cK] \\ T_\tau \\ [mm] \\ \mu_\tau^S \\ [cK] \\ \mu_\tau^T \end{bmatrix} + \begin{bmatrix} [mm] \\ \epsilon_\tau^S \\ [cK] \\ \epsilon_\tau^T \end{bmatrix}. \tag{57}$$

D Tables

In this section we report the tables with the results for the model comparison forecasting exercise and the parameter estimates for models 1-2 and models 3-4. See Sections 4 and 6 for more details.

Table 1: Ratios between R_f^1 and R_f^j, $j = 1, \ldots, 12$.

n^*	1535	1510	1485	1460	1435	1410	1385	1360	1335	1310
f	25	50	75	100	125	150	175	200	225	250
model 1	1,00	1,00	1,00	1,00	1,00	1,00	1,00	1,00	1,00	1,00
model 2	1,00	1,02	1,02	1,00	1,01	1,04	**0,89**	1,06	1,03	1,02
model 3	**0,99**	1,10	1,08	1,03	1,01	1,03	1,02	1,00	1,02	1,03
model 4	**0,99**	1,09	1,07	1,02	**0,99**	**0,99**	1,02	**0,9**	**0,97**	1,03
model 5	1,07	1,00	1,31	1,21	1,19	1,24	1,06	**0,75**	1,09	1,04
model 6	1,06	**0,98**	1,26	1,17	1,07	**0,82**	**0,62**	1,01	**0,56**	**0,5**
model 7	**0,7**	1,26	1,24	1,09	1,17	1,14	**0,76**	**0,55**	1,01	**0,97**
model 8	**0,7**	1,25	1,22	1,08	1,15	1,22	1,19	1,15	1,03	**0,9**
model 9	1,07	1,00	1,31	1,21	1,19	1,24	1,06	**0,75**	1,09	1,04
model 10	1,06	**0,99**	1,26	1,17	**0,98**	**0,99**	**0,77**	1,16	**0,75**	**0,66**
model 11	**0,7**	1,24	1,21	1,01	1,02	**0,89**	**0,52**	**0,38**	**0,56**	**0,54**
model 12	**0,7**	1,22	1,17	**0,99**	1,00	1,18	**0,87**	**0,73**	**0,97**	1,02

n^*	1535	1510	1485	1460	1435	1410	1385	1360	1335	1310
f	25	50	75	100	125	150	175	200	225	250
model 1	1,00	1,00	1,00	1,00	1,00	1,00	1,00	1,00	1,00	1,00
model 2	1,04	1,05	**0,91**	1,00	**0,98**	**0,91**	**0,9**	**0,99**	**0,94**	**0,97**
model 3	1,14	1,09	**0,7**	**0,76**	1,28	1,10	1,23	1,04	1,42	1,85
model 4	1,12	1,17	**0,78**	**0,85**	1,36	1,21	1,37	1,12	1,59	2,03
model 5	1,12	1,05	**0,31**	**0,31**	**0,67**	**0,5**	**0,48**	**0,46**	**0,67**	**0,96**
model 6	**0,87**	**0,68**	**0,31**	**0,31**	**0,59**	**0,52**	**0,49**	**0,46**	**0,67**	1,02
model 7	1,19	**0,6**	**0,38**	**0,36**	**0,57**	**0,51**	**0,68**	**0,87**	1,03	1,29
model 8	**0,91**	**0,51**	**0,38**	**0,35**	**0,54**	**0,48**	**0,62**	**0,78**	**0,97**	1,17
model 9	1,12	1,05	**0,31**	**0,31**	**0,67**	**0,5**	**0,48**	**0,46**	**0,67**	**0,96**
model 10	1,11	1,09	**0,4**	**0,41**	**0,9**	**0,8**	**0,71**	**0,66**	**0,97**	1,89
model 11	**0,85**	1,14	**0,59**	**0,66**	1,23	1,21	1,63	1,43	1,42	1,80
model 12	1,10	1,08	**0,71**	**0,75**	1,24	1,09	1,48	1,53	1,36	1,91

Ratios between R_f^1 (performance measure (35) for model 1) and R_f^j (performance measure (35) for model j), $j = 1, \ldots, 12$ for different values of n^* (the length of the estimation sample) and f (the number of out-of-sample forecasts). See Section 4.1 for more details on the forecasting procedure. The complete dataset is made up of $n = n^* + f = 1560$ observations, ranging from January 1880 to December 2009.

Table 2: Ratios between R_f^2 and R_f^j, $j = 1, \ldots, 12$.

n^*	1535	1510	1485	1460	1435	1410	1385	1360	1335	1310
f	25	50	75	100	125	150	175	200	225	250
model 1	1,00	**0,98**	**0,98**	1,00	**0,99**	**0,96**	1,12	**0,94**	**0,98**	**0,98**
model 2	1,00	1,00	1,00	1,00	1,00	1,00	1,00	1,00	1,00	1,00
model 3	**0,99**	1,08	1,05	1,03	1,00	**0,98**	1,14	**0,94**	1,00	1,01
model 4	**0,99**	1,07	1,04	1,02	**0,98**	**0,95**	1,14	**0,84**	**0,95**	1,01
model 5	1,07	**0,98**	1,28	1,20	1,17	1,19	1,19	**0,71**	1,07	1,02
model 6	1,06	**0,96**	1,23	1,17	1,06	**0,78**	**0,7**	**0,95**	**0,54**	**0,49**
model 7	**0,7**	1,23	1,21	1,09	1,15	1,09	**0,85**	**0,52**	**0,99**	**0,95**
model 8	**0,7**	1,23	1,20	1,08	1,14	1,17	1,34	1,08	1,00	**0,89**
model 9	1,07	**0,98**	1,28	1,20	1,17	1,19	1,19	**0,71**	1,07	1,02
model 10	1,06	**0,97**	1,24	1,16	**0,97**	**0,95**	**0,87**	1,09	**0,73**	**0,65**
model 11	**0,7**	1,22	1,18	1,01	1,00	**0,85**	**0,58**	**0,36**	**0,55**	**0,53**
model 12	**0,7**	1,19	1,14	**0,99**	**0,99**	1,13	**0,98**	**0,69**	**0,94**	1,00

n^*	1535	1510	1485	1460	1435	1410	1385	1360	1335	1310
f	25	50	75	100	125	150	175	200	225	250
model 1	**0,96**	**0,95**	1,10	1,00	1,02	1,10	1,11	1,01	1,06	1,03
model 2	1,00	1,00	1,00	1,00	1,00	1,00	1,00	1,00	1,00	1,00
model 3	1,10	1,04	**0,77**	**0,76**	1,30	1,21	1,37	1,05	1,51	1,91
model 4	1,07	1,12	**0,86**	**0,85**	1,39	1,33	1,52	1,13	1,69	2,09
model 5	1,07	1,00	**0,34**	**0,31**	**0,68**	**0,55**	**0,53**	**0,46**	**0,71**	**0,98**
model 6	**0,83**	**0,65**	**0,34**	**0,31**	**0,6**	**0,58**	**0,55**	**0,46**	**0,71**	1,05
model 7	1,14	**0,57**	**0,42**	**0,36**	**0,58**	**0,57**	**0,76**	**0,87**	1,10	1,33
model 8	**0,87**	**0,49**	**0,42**	**0,35**	**0,55**	**0,53**	**0,69**	**0,79**	1,03	1,20
model 9	1,07	1,00	**0,34**	**0,31**	**0,68**	**0,55**	**0,54**	**0,46**	**0,71**	**0,99**
model 10	1,07	1,03	**0,44**	**0,41**	**0,92**	**0,88**	**0,79**	**0,67**	1,03	1,95
model 11	**0,82**	1,08	**0,64**	**0,66**	1,25	1,33	1,81	1,44	1,51	1,86
model 12	1,06	1,03	**0,78**	**0,75**	1,26	1,20	1,65	1,54	1,44	1,97

Ratios between R_f^2 (performance measure (35) for model 2) and R_f^j (performance measure (35) for model j), $j = 1, \ldots, 12$ for different values of n^* (the length of the estimation sample) and f (the number of out-of-sample forecasts). See Section 4.1 for more details on the forecasting procedure. The complete dataset is made up of $n = n^* + f = 1560$ observations, ranging from January 1880 to December 2009.

Table 3: Ratios between R_f^3 and R_f^j, $j = 1, \ldots, 12$.

n^*	1535	1510	1485	1460	1435	1410	1385	1360	1335	1310
f	25	50	75	100	125	150	175	200	225	250
model 1	1,01	**0,91**	**0,93**	**0,97**	**0,99**	**0,97**	**0,98**	1,00	**0,98**	**0,97**
model 2	1,01	**0,93**	**0,95**	**0,97**	1,00	1,02	**0,88**	1,06	1,00	**0,99**
model 3	1,00	1,00	1,00	1,00	1,00	1,00	1,00	1,00	1,00	1,00
model 4	1,00	1,00	**0,99**	**0,99**	**0,98**	**0,96**	1,00	**0,9**	**0,95**	1,00
model 5	1,07	**0,91**	1,22	1,17	1,17	1,21	1,04	**0,75**	1,07	1,01
model 6	1,07	**0,9**	1,17	1,13	1,06	**0,8**	**0,61**	1,01	**0,54**	**0,48**
model 7	**0,71**	1,15	1,15	1,06	1,15	1,11	**0,75**	**0,55**	**0,99**	**0,95**
model 8	**0,71**	1,14	1,14	1,04	1,14	1,19	1,17	1,15	1,01	**0,88**
model 9	1,07	**0,91**	1,22	1,17	1,17	1,21	1,04	**0,75**	1,07	1,01
model 10	1,07	**0,9**	1,18	1,13	**0,97**	**0,96**	**0,76**	1,16	**0,73**	**0,65**
model 11	**0,71**	1,13	1,13	**0,98**	1,00	**0,86**	**0,51**	**0,38**	**0,55**	**0,52**
model 12	**0,71**	1,11	1,09	**0,96**	**0,98**	1,15	**0,86**	**0,73**	**0,95**	**0,99**

n^*	1285	1260	1235	1210	1185	1160	1135	1110	1085	1060
f	275	300	325	350	375	400	425	450	475	500
model 1	**0,87**	**0,91**	1,42	1,31	**0,78**	**0,91**	**0,81**	**0,96**	**0,7**	**0,54**
model 2	**0,91**	**0,96**	1,30	1,31	**0,77**	**0,83**	**0,73**	**0,95**	**0,66**	**0,52**
model 3	1,00	1,00	1,00	1,00	1,00	1,00	1,00	1,00	1,00	1,00
model 4	**0,98**	1,07	1,11	1,12	1,07	1,10	1,11	1,07	1,12	1,10
model 5	**0,98**	**0,96**	**0,44**	**0,4**	**0,52**	**0,45**	**0,39**	**0,44**	**0,47**	**0,52**
model 6	**0,76**	**0,62**	**0,45**	**0,4**	**0,46**	**0,47**	**0,4**	**0,44**	**0,47**	**0,55**
model 7	1,04	**0,54**	**0,54**	**0,48**	**0,45**	**0,47**	**0,56**	**0,83**	**0,73**	**0,7**
model 8	**0,8**	**0,47**	**0,54**	**0,46**	**0,42**	**0,44**	**0,5**	**0,75**	**0,68**	**0,63**
model 9	**0,98**	**0,96**	**0,44**	**0,4**	**0,52**	**0,45**	**0,39**	**0,44**	**0,47**	**0,52**
model 10	**0,97**	**0,99**	**0,57**	**0,54**	**0,71**	**0,72**	**0,58**	**0,63**	**0,68**	1,02
model 11	**0,75**	1,04	**0,84**	**0,86**	**0,96**	1,10	1,32	1,37	1,00	**0,97**
model 12	**0,97**	**0,99**	1,01	**0,98**	**0,97**	**0,99**	1,20	1,46	**0,96**	1,03

Ratios between R_f^3 (performance measure (35) for model 3) and R_f^j (performance measure (35) for model j), $j = 1, \ldots, 12$ for different values of n^* (the length of the estimation sample) and f (the number of out-of-sample forecasts). See Section 4.1 for more details on the forecasting procedure. The complete dataset is made up of $n = n^* + f = 1560$ observations, ranging from January 1880 to December 2009.

Table 4: Ratios between R_f^4 and R_f^j, $j = 1, \ldots, 12$.

n^*	1535	1510	1485	1460	1435	1410	1385	1360	1335	1310
f	25	50	75	100	125	150	175	200	225	250
model 1	1,01	**0,92**	**0,94**	**0,98**	1,01	1,01	**0,98**	1,12	1,03	**0,97**
model 2	1,01	**0,93**	**0,96**	**0,98**	1,02	1,06	**0,88**	1,18	1,06	**0,99**
model 3	1,00	1,00	1,01	1,01	1,03	1,04	1,00	1,12	1,06	1,00
model 4	1,00	1,00	1,00	1,00	1,00	1,00	1,00	1,00	1,00	1,00
model 5	1,07	**0,91**	1,23	1,18	1,20	1,26	1,04	**0,84**	1,13	1,01
model 6	1,07	**0,9**	1,18	1,14	1,08	**0,83**	**0,61**	1,12	**0,57**	**0,48**
model 7	**0,71**	1,15	1,16	1,07	1,18	1,15	**0,75**	**0,61**	1,05	**0,95**
model 8	**0,71**	1,15	1,15	1,05	1,16	1,24	1,17	1,28	1,06	**0,88**
model 9	1,07	**0,91**	1,23	1,18	1,20	1,26	1,04	**0,84**	1,13	1,01
model 10	1,07	**0,9**	1,19	1,14	**0,99**	1,00	**0,76**	1,30	**0,77**	**0,64**
model 11	**0,71**	1,14	1,14	**0,99**	1,03	**0,9**	**0,51**	**0,42**	**0,58**	**0,52**
model 12	**0,71**	1,11	1,09	**0,97**	1,01	1,19	**0,86**	**0,82**	1,00	**0,99**

n^*	1535	1510	1485	1460	1435	1410	1385	1360	1335	1310
f	25	50	75	100	125	150	175	200	225	250
model 1	**0,89**	**0,85**	1,28	1,17	**0,73**	**0,83**	**0,73**	**0,89**	**0,63**	**0,49**
model 2	**0,93**	**0,9**	1,17	1,17	**0,72**	**0,75**	**0,66**	**0,88**	**0,59**	**0,48**
model 3	1,02	**0,93**	**0,9**	**0,9**	**0,94**	**0,91**	**0,9**	**0,93**	**0,9**	**0,91**
model 4	1,00	1,00	1,00	1,00	1,00	1,00	1,00	1,00	1,00	1,00
model 5	1,00	**0,89**	**0,4**	**0,36**	**0,49**	**0,41**	**0,35**	**0,41**	**0,42**	**0,47**
model 6	**0,78**	**0,58**	**0,4**	**0,36**	**0,43**	**0,43**	**0,36**	**0,41**	**0,42**	**0,5**
model 7	1,06	**0,51**	**0,49**	**0,43**	**0,42**	**0,43**	**0,5**	**0,77**	**0,65**	**0,64**
model 8	**0,81**	**0,44**	**0,49**	**0,41**	**0,4**	**0,4**	**0,45**	**0,7**	**0,61**	**0,58**
model 9	1,00	**0,9**	**0,4**	**0,36**	**0,49**	**0,41**	**0,35**	**0,41**	**0,42**	**0,47**
model 10	**0,99**	**0,92**	**0,51**	**0,49**	**0,66**	**0,66**	**0,52**	**0,59**	**0,61**	**0,93**
model 11	**0,76**	**0,97**	**0,75**	**0,77**	**0,9**	1,00	1,19	1,28	**0,9**	**0,89**
model 12	**0,99**	**0,92**	**0,91**	**0,87**	**0,91**	**0,9**	1,08	1,36	**0,86**	**0,94**

Ratios between R_f^4 (performance measure (35) for model 4) and R_f^j (performance measure (35) for model j), $j = 1, \ldots, 12$ for different values of n^* (the length of the estimation sample) and f (the number of out-of-sample forecasts). See Section 4.1 for more details on the forecasting procedure. The complete dataset is made up of $n = n^* + f = 1560$ observations, ranging from January 1880 to December 2009.

Table 5: Parameter estimates for model 1-2.

(a) Continuous-time, model 1-2, parameter estimates.

	σ^T $[cK]$	a^{SS} $[\frac{1}{month}]$	a^{ST} $[\frac{mm}{cK \cdot month}]$	a^{TS} $\left[\frac{cK}{mm \cdot month}\right]$	a^{TT} $[\frac{1}{month}]$
value	7,59	-0,0112	0,0056	0,0512	-0,0816
std.	(0,2311)	(0,0016)	(0,002)	(0,0075)	(0,0075)
t-ratio	[32,84]	[-7]	[2,8]	[6,83]	[-10,88]

	λ_l^S $[\frac{mm}{month}]$	λ_l^T $\left[\frac{cK}{month}\right]$	$\sqrt{\Sigma^{SS}}$ $\left[\frac{mm}{\sqrt{month}}\right]$	Σ^{ST} $\left[\frac{mm \cdot cK}{month}\right]$	$\sqrt{\Sigma^{TT}}$ $\left[\frac{cK}{\sqrt{month}}\right]$
value	0,0012	-0,0022	1,11	0,34	5,87
std.	(0,0001)	(0,0008)	(0,1151)	(0,3733)	(0,2703)
t-ratio	[12]	[-2,75]	[9,64]	[0,91]	[21,72]

Parameter estimates for model 1-2 in the continuous-time representation (equations (22), (24), and (32)). Standard deviations are reported in parentheses, and the t-ratios in square brackets. The parameters were estimated using information from time $t = 1$ (January 1880) to time $t = n$ (December 2009). The standard deviations were obtained from the bootstrap procedure described in Appendix B.

(b) Continuous-time, model 1-2, parameter estimates (alternative measurement units).

	σ^T $[K]$	a^{SS} $\left[\frac{1}{year}\right]$	a^{ST} $[\frac{mm}{cK \cdot month}]$	a^{TS} $\left[\frac{cK}{mm \cdot month}\right]$	a^{TT} $\left[\frac{1}{year}\right]$
value	0,0759	-0,1344	0,00672	6,144	-0,9792

	λ_l^S $\left[\frac{m}{year}\right]$	λ_l^T $\left[\frac{K}{year}\right]$	$\sqrt{\Sigma^{SS}}$ $\left[\frac{m}{\sqrt{year}}\right]$	Σ^{ST} $\left[\frac{m \cdot K}{year}\right]$	$\sqrt{\Sigma^{TT}}$ $\left[\frac{K}{\sqrt{year}}\right]$
value	0,000014	-0,00026	0,0038	0,000041	0,20

Parameter estimates for model 1-2 in the continuous-time representation (equations (22), (24), and (32)). The parameters were estimated using information from time $t = 1$ (January 1880) to time $t = n$ (December 2009).

Table 6: Parameter estimates for model 1-2.

(a) Discrete-time, model 1-2, parameter estimates.

	σ^T	$A^{*,SS}$	$A^{*,ST}$	$A^{*,S\mu^S}$	$A^{*,S\mu^T}$	$A^{*,TS}$	$A^{*,TT}$	$A^{*,T\mu^S}$
	$[cK]$		$\left[\frac{mm}{cK}\right]$		$\left[\frac{mm}{cK}\right]$	$\left[\frac{cK}{mm}\right]$		$\left[\frac{cK}{mm}\right]$
value	7,59	0,99	0,0054	0,99	0,0027	0,0489	0,92	0,0248
std.	(0,2311)	(0,0015)	(0,0019)	(0,0008)	(0,001)	(0,007)	(0,0068)	(0,0036)
t-ratio	[32,82]	[641,96]	[2,86]	[1275,33]	[2,86]	[6,98]	[135,24]	[6,92]

	$A^{*,T\mu^T}$	c^S $[mm]$	c^T $[cK]$	c^{μ^S} $[mm]$	c^{μ^T} $[cK]$	$\sqrt{\Sigma^{*,SS}}$ $[mm]$	$\Sigma^{*,ST}$ $[mm \cdot cK]$	$\sqrt{\Sigma^{*,TT}}$ $[cK]$
value	0,96	0,0006	-0,001	0,0012	-0,0022	1,11	0,44	5,64
std.	(0,0035)	(0,0001)	(0,0004)	(0,0001)	(0,0008)	(0,1108)	(0,3661)	(0,2535)
t-ratio	[273,14]	[8,28]	[-2,56]	[8,25]	[-2,57]	[9,98]	[1,21]	[22,24]

Parameter estimates for model 1-2 in the dicrete-time representation (equations (34)). Standard deviations are reported in parentheses, and the t-ratios in square brackets. The parameters were estimated using information from time $t = 1$ (January 1880) to time $t = n$ (December 2009). The standard deviations were obtained from the bootstrap procedure described in Appendix B.

(b) Discrete-time, model 1-2, parameter estimates (alternative measurement units).

	σ^T	$A^{*,SS}$	$A^{*,ST}$	$A^{*,S\mu^S}$	$A^{*,S\mu^T}$	$A^{*,TS}$	$A^{*,TT}$	$A^{*,T\mu^S}$
	$[K]$		$\left[\frac{m}{K}\right]$		$\left[\frac{m}{K}\right]$	$\left[\frac{K}{m}\right]$		$\left[\frac{K}{m}\right]$
value	0,0759	0,99	0,00054	0,99	0,00027	0,489	0,92	0,248

	$A^{*,T\mu^T}$	c^S $[m]$	c^T $[K]$	c^{μ^S} $[m]$	c^{μ^T} $[K]$	$\sqrt{\Sigma^{*,SS}}$ $[m]$	$\Sigma^{*,ST}$ $[m \cdot K]$	$\sqrt{\Sigma^{*,TT}}$ $[K]$
value	0,96	0,0000006	-0,00001	0,0000012	-0,000022	0,00111	0,0000044	0,0564

Parameter estimates for model 1-2 in the discrete-time representation (equations (34)). The parameters were estimated using information from time $t = 1$ (January 1880) to time $t = n$ (December 2009).

Table 7: Parameter estimates for model 3-4.

(a) Continuous-time, model 3-4, parameter estimates.

	σ^T $[cK]$	a^{SS} $\left[\frac{1}{month}\right]$	a^{ST} $\left[\frac{mm}{cK \cdot month}\right]$	a^{TS} $\left[\frac{cK}{mm \cdot month}\right]$	a^{TT} $\left[\frac{1}{month}\right]$
value	7,41	-0,0288	-0,0037	-0,0458	-0,1169
std.	(0,27)	(0,0014)	(0,0026)	(0,006)	(0,0106)
t-ratio	[27,44]	[-20,57]	[-1,42]	[-7,63]	[-11,03]

	λ_q^S $\left[\frac{mm}{month^3}\right]$	λ_q^T $\left[\frac{cK}{month^3}\right]$	$\sqrt{\Sigma^{SS}}$ $\left[\frac{mm}{\sqrt{month}}\right]$	Σ^{ST} $\left[\frac{mm \cdot cK}{month}\right]$	$\sqrt{\Sigma^{TT}}$ $\left[\frac{cK}{\sqrt{month}}\right]$
value	0,000003	0,000015	1,25	1,46	5,91
std.	(0,0000004)	(0,000002)	(0,19)	(0,47)	(0,30)
t-ratio	[7,5]	[7,5]	[6,43]	[3,12]	[19,97]

Parameter estimates for model 3-4 in the continuous-time representation (equations (22), (25), and (32)). Standard deviations are reported in parentheses, and the t-ratios in square brackets. The parameters were estimated using information from time $t = 1$ (January 1880) to time $t = n$ (December 2009). The standard deviations were obtained from the bootstrap procedure described in Appendix B.

(b) Continuous-time, model 3-4, parameter estimates (alternative measurement units).

	σ^T $[K]$	a^{SS} $\left[\frac{1}{year}\right]$	a^{ST} $\left[\frac{m}{K \cdot year}\right]$	a^{TS} $\left[\frac{K}{m \cdot year}\right]$	a^{TT} $\left[\frac{1}{year}\right]$
value	0,0741	-0,3456	-0,00444	-5,496	-1,4028

	λ_q^S $\left[\frac{m}{year^3}\right]$	λ_q^T $\left[\frac{K}{year^3}\right]$	$\sqrt{\Sigma^{SS}}$ $\left[\frac{m}{\sqrt{year}}\right]$	Σ^{ST} $\left[\frac{m \cdot K}{year}\right]$	$\sqrt{\Sigma^{TT}}$ $\left[\frac{K}{\sqrt{year}}\right]$
value	0,00000043	0,000021	0,0043	0,00018	0,20

Parameter estimates for model 3-4 in the continuous-time representation (equations (22), (25), and (32)). The parameters were estimated using information from time $t = 1$ (January 1880) to time $t = n$ (December 2009).

Table 8: Discrete-time, model 3-4, parameter estimates.

	σ^T $[cK]$	$A^{*,SS}$	$A^{*,ST}$ $\left[\frac{mm}{cK}\right]$	$A^{*,S\mu^S}$	$A^{*,S\mu^T}$ $\left[\frac{mm}{cK}\right]$	$A^{*,S\lambda^S}$ $[month]$
value	7,41	0,97	-0,0035	0,99	-0,0018	0,4952
std.	(0,27)	(0,0013)	(0,0024)	(0,0007)	(0,0012)	(0,0002)
t-ratio	[27,44]	[746,15]	[-1,46]	[1414,29]	[-1,5]	[2476]

	$A^{*,S\lambda^T}$ $\left[\frac{month\cdot mm}{cK}\right]$	$A^{*,TS}$ $\left[\frac{cK}{mm}\right]$	$A^{*,TT}$	$A^{*,T\mu^S}$ $\left[\frac{cK}{mm}\right]$	$A^{*,T\mu^T}$	$A^{*,T\lambda^S}$ $\left[\frac{month\cdot cK}{mm}\right]$
value	-0,0006	-0,0426	0,89	-0,0218	0,94	-0,0074
std.	(0,0004)	(0,0053)	(0,0092)	(0,0028)	(0,0048)	(0,0009)
t-ratio	[-1,5]	[-8,04]	[96,74]	[-7,79]	[196,63]	[-8,22]

	$A^{*,T\lambda^T}$ $[month]$	c^S $[mm]$	c^T $[cK]$	c^{μ^S} $[mm]$	c^{μ^T} $[cK]$
value	0,4811	0	0,000002	0,000001	0,000007
std.	(0,0016)	(0,00000007)	(0,00000039)	(0,0000002)	(0,000001)
t-ratio	[300,69]	[6,29]	[6,05]	[6,65]	[7,32]

	c^{λ^S} $\left[\frac{mm}{month}\right]$	c^{λ^T} $\left[\frac{cK}{month}\right]$	$\sqrt{\Sigma^{*,SS}}$ $[mm]$	$\Sigma^{*,ST}$ $[mm\cdot cK]$	$\sqrt{\Sigma^{*,TT}}$ $[cK]$
value	0,000003	0,000015	1,25	1,46	5,91
std.	(0,0000004)	(0,000002)	(0,19)	(0,47)	(0,3)
t-ratio	[6,63]	[7,32]	[6,58]	[3,11]	[19,7]

Parameter estimates for model 3-4 in the discrete-time representation (equations (22), (25), and (32)). Standard deviations are reported in parentheses, and the t-ratios in square brackets. The parameters were estimated using information from time $t = 1$ (January 1880) to time $t = n$ (December 2009). The standard deviations were obtained from the bootstrap procedure described in Appendix B.

Table 9: Discrete-time, model 3-4, parameter estimates (alternative measurement units).

	σ^T $[K]$	$A^{*,SS}$	$A^{*,ST}$ $\left[\frac{m}{K}\right]$	$A^{*,S\mu^S}$	$A^{*,S\mu^T}$ $\left[\frac{m}{K}\right]$	$A^{*,S\lambda^S}$ $[year]$
value	0,074	0,97	-0,00035	0,99	-0,00018	0,041

	$A^{*,S\lambda^T}$ $\left[\frac{year \cdot m}{K}\right]$	$A^{*,TS}$ $\left[\frac{K}{m}\right]$	$A^{*,TT}$	$A^{*,T\mu^S}$ $\left[\frac{K}{m}\right]$	$A^{*,T\mu^T}$	$A^{*,T\lambda^S}$ $\left[\frac{year \cdot K}{m}\right]$
value	-0,000005	-0,426	0,89	-0,218	0,94	-0,0062

	$A^{*,T\lambda^T}$ $[year]$	c^S $[m]$	c^T $[K]$	c^{μ^S} $[m]$	c^{μ^T} $[K]$	
value	0,040	0	0,00000002	0,000000001	0,00000007	

	c^{λ^S} $\left[\frac{m}{year}\right]$	c^{λ^T} $\left[\frac{K}{year}\right]$	$\sqrt{\Sigma^{*,SS}}$ $[m]$	$\Sigma^{*,ST}$ $[m \cdot K]$	$\sqrt{\Sigma^{*,TT}}$ $[K]$	
value	0,000000036	0,0000018	0,0013	0,000014	0,0591	

Parameter estimates for model 3-4 in the discrete-time representation (equations (22), (25), and (32)). The parameters were estimated using information from time $t = 1$ (January 1880) to time $t = n$ (December 2009).

Research Papers 2013

2015-23: Eric Hillebrand, Søren Johansen and Torben Schmith: Data revisions and the statistical relation of global mean sea-level and temperature

2015-24: Tommaso Proietti and Alessandra Luati: Generalised partial autocorrelations and the mutual information between past and future

2015-25: Bent Jesper Christensen and Rasmus T. Varneskov: Medium Band Least Squares Estimation of Fractional Cointegration in the Presence of Low-Frequency Contamination

2015-26: Ulrich Hounyo and Rasmus T. Varneskov: A Local Stable Bootstrap for Power Variations of Pure-Jump Semimartingales and Activity Index Estimation

2015-27: Rasmus Søndergaard Pedersen and Anders Rahbek: Nonstationary ARCH and GARCH with t-distributed Innovations

2015-28: Tommaso Proietti and Eric Hillebrand: Seasonal Changes in Central England Temperatures

2015-29: Laurent Callot and Johannes Tang Kristensen: Regularized Estimation of Structural Instability in Factor Models: The US Macroeconomy and the Great Moderation

2015-30: Davide Delle Monache, Stefano Grassi and Paolo Santucci de Magistris: Testing for Level Shifts in Fractionally Integrated Processes: a State Space Approach

2015-31: Matias D. Cattaneo, Michael Jansson and Whitney K. Newey: Treatment Effects with Many Covariates and Heteroskedasticity

2015-32: Jean-Guy Simonato and Lars Stentoft: Which pricing approach for options under GARCH with non-normal innovations?

2015-33: Nina Munkholt Jakobsen and Michael Sørensen: Efficient Estimation for Diffusions Sampled at High Frequency Over a Fixed Time Interval

2015-34: Wei Wei and Denis Pelletier: A Jump-Diffusion Model with Stochastic Volatility and Durations

2015-35: Yunus Emre Ergemen and Carlos Velasco: Estimation of Fractionally Integrated Panels with Fixed Effects and Cross-Section Dependence

2015-36: Markku Lanne and Henri Nyberg: Nonlinear dynamic interrelationships between real activity and stock returns

2015-37: Markku Lanne and Jani Luoto: Estimation of DSGE Models under Diffuse Priors and Data-Driven Identification Constraints

2015-38: Lorenzo Boldrini and Eric Hillebrand: Supervision in Factor Models Using a Large Number of Predictors

2015-39: Lorenzo Boldrini and Eric Hillebrand: The Forecasting Power of the Yield Curve, a Supervised Factor Model Approach

2015-40: Lorenzo Boldrini: Forecasting the Global Mean Sea Level, a Continuous-Time State-Space Approach